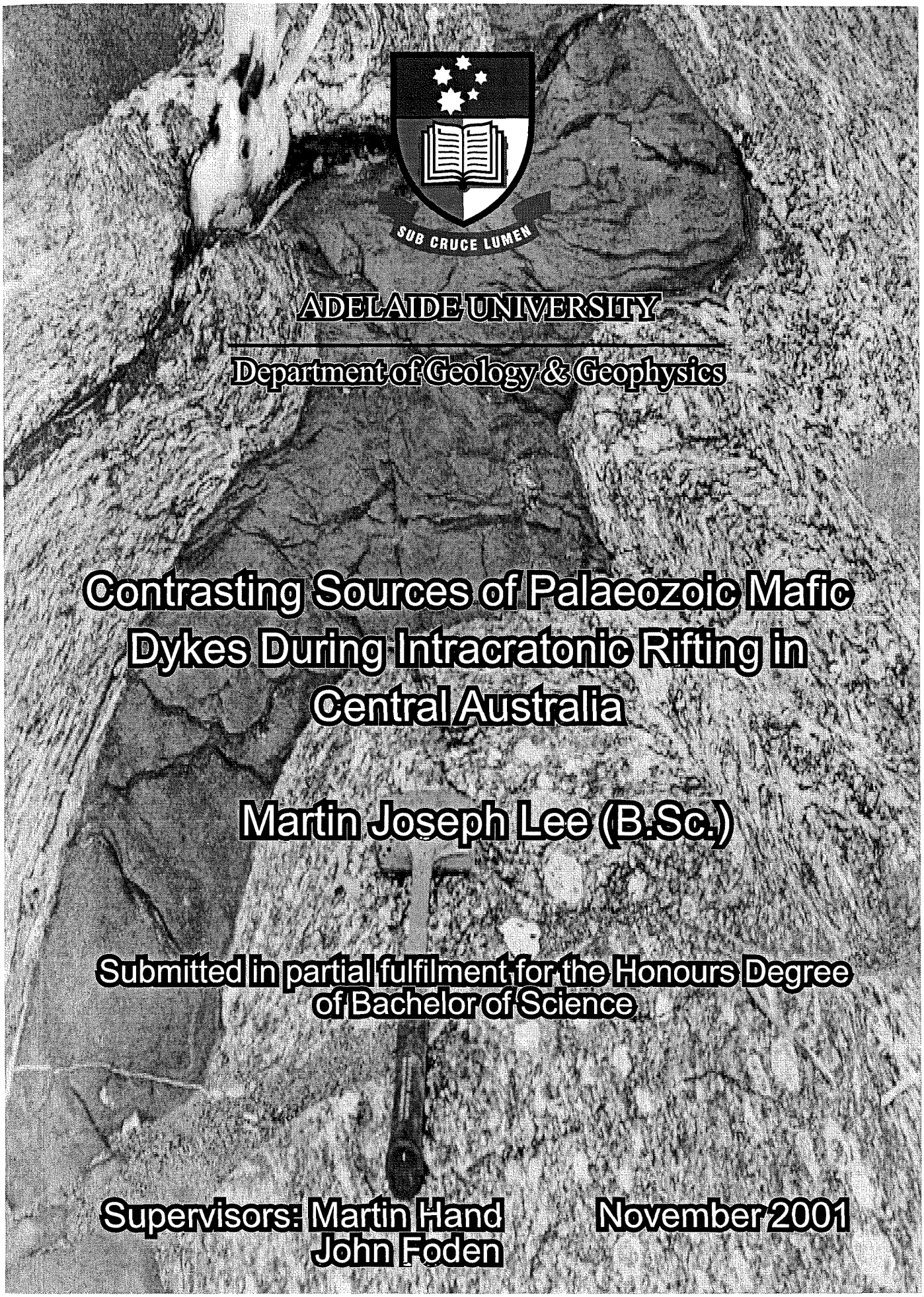

ADELAIDE UNIVERSITY

Department of Geology & Geophysics

Contrasting Sources of Palaeozoic Mafic Dykes During Intracratonic Rifting in Central Australia

Martin Joseph Lee (B.Sc.)

Submitted in partial fulfilment for the Honours Degree of Bachelor of Science

Supervisors: Martin Hand
John Foden

November 2001

TABLE OF CONTENTS

LIST OF TABLES

LIST OF FIGURES

STATEMENT

This work contains no material which has been accepted for the award of any other degree or diploma in any other university or tertiary institution. To the best of my knowledge this investigation contains no material previously published or written by another person, except where due reference has be made in the text.

I give consent for this copy of my manuscript, when received by the Barr Smith Library or University, to be available for loan and/or photocopying.

Martin Joseph Lee B.Sc.

ACKNOWLEDGEMENTS

The work contained in this manuscript could not have been possible without the efforts of the following people:

Firstly to Martin Hand. My deepest thanks go to him for the opportunities he has presented me with this year. A special thanks for his monetary support during periods of fieldwork and chemical analysis. His knowledge, support, enthusiasm for geology and tiresome work has been a priceless asset and welcomed source of motivation.

I would also like to thank John Foden for his geochemical expertise, ongoing advice and assistance in the field. Thanks must also be given to Karin Barovich for the insightful comments and suggestions made during data analysis and interpretation. David Bruce, Wayne Mussared and John Stanley are all thanked for their expertise during data collation.

I also give a vote of thanks to fellow colleague Mark Rieuwers for his arduous assistance, company and patience whilst in the field. Ben Wade is also thanked for the assistance he has provided in the laboratory and during writing.

Last, but by no means least: Mum, Dad and Catherine are all especially thanked for the love, moral support and advice they have given to me…it is greatly appreciated.

Abstract

The rift-related Cambro-Ordovician Harts Range Metamorphic Complex, in the eastern Arunta Block, central Australia, contains a suite of early Ordovician meta-basaltic rocks (the Harts Range Dykes) that were emplaced syn-kinematically into low-angle regional-scale ductile extensional detachment zones that accommodated N-S extension. The early Ordovician extension was coeval with the deposition of the Larapinta Group in the Amadeus Basin, and was associated with development of the Larapintine Seaway, which linked Australia's eastern margin to the Canning Basin.

Major element variation within the dykes is consistent with an evolutionary path dominated by olivine, and to a lesser extent clinopyroxene and plagioclase fractionation. Based on trace element and isotopic criteria, the dykes have been subdivided into two suites: the Group 1 and 2 dykes. This subdivision is evident in discrimination diagrams, which assign them to a variety of petrological settings, despite the knowledge of their emplacement within an intracratonic rift. These diagrams suggest that the Group 1 dykes have N-type MORB affinities, while Group 2 dykes were derived from E-type MORB or volcanic/island arc sources.

The Group 1 dykes are characterised by higher Zr and Y but lower Nb, Ba, La, Ni, Cr and Ce values than those of the Group 2 dykes. High Zr/Nb ratio values of 62 for the Group 1 dykes suggest they were derived from a depleted source, as does the near flat REE pattern, $(La/Yb)_N$ = 1.21, which is N-type MORB like. The Group 1 dykes have positive $\varepsilon_{Nd}(480)$ values associated with less contaminated, depleted signatures. The Group 2 dykes have lower Zr and Y, but higher Nb, Ba, La, Ni, Cr and Ce compositions than the Group 1 dykes, and have Zr/Nb ratio values of 14, indicating an arc-like source. They also display a slightly LREE enriched pattern $(La/Yb)_N$ = 5.12, similar to that of E-type MORB. The low and variable $\varepsilon_{Nd}(480)$ values –11.5, -2.1 and 0 and extremely high $(^{87}Sr/^{86}Sr)_i$ values of the Group 2 dykes suggests varying degrees of enrichment.

The $\varepsilon_{Nd}(480)$ values and variations in Nd and Sr concentrations in the Harts Range Dykes provide evidence for multiple magma sources. Geochemical and isotopic data suggest that the Group 1 dykes have upper asthenospheric, depleted mantle characteristics similar to other meta-tholeiites in the Harts Range region. The enriched geochemical signature of the Group 2 dykes may reflect contamination by a metasomatised mafic crust. However, a subduction-modified and chemically isolated continental lithospheric mantle source is preferred, because of the close-fit comparison in trace element data with a similarly interpreted adjacent suite of dykes. The bulk average continental lithospheric mantle (CLM) is ruled out as a dominant source for the enriched chemical signature of the Group 2 dykes, because it does not exhibit the HFS-element depleted and LIL-element enriched character of a subduction-modified continental lithospheric mantle. Additionally, the Group 2 dykes have higher incompatible element compositions than the bulk average CLM.

Keywords: Cambro-Ordovician; central Australia; intracraonic rift; Harts Range Dykes; N-type MORB; CLM

1. Introduction

A common fundamental feature of continental rifting is mafic magmatism which samples the evolving lithospheric and asthenospheric mantle. The compositional range and variation of rift-related basaltic rocks provide crucial data for understanding the processes involved in extension of continental lithosphere (e.g. Zwaan and Van Roermund, 1990; Baldridge et al., 1991; Gibson et al., 1996).

The difficulty in studying mafic rocks emplaced in continental rifts is the uncertainty of identifying contributing sources of melt. At mid-ocean ridges it is obvious that the rocks sample the upper depleted asthenosphere (Stakes et al., 1984), and ocean island settings such as Hawaii are known ocean island provinces (Sun and McDonough, 1989). In continental settings, melts generated in the continental lithospheric mantle or in the underlying asthenosphere will experience various degrees of interaction with the continental crust during ascension and emplacement. The overlying presence of the continental crust generates the geochemical ambiguity of rift style magmas. The mantle source region of continental rift-related mafic magmas has been a major issue in many recent studies (e.g. Baldridge et al., 1991; Rochell et al., 1995; Baker et al., 1996a). Whether or not magmas are derived from the continental lithospheric mantle or from sub-lithospheric sources such as the asthenosphere or in mantle plumes is also of primary concern (Paslick et al., 1995; Spath et al., 2001). Below are three possible sources for intracratonic rift-related melts:

(1) Plume sources: Most geochemical studies of magmas from major continental rifts have focussed on flood basalts (e.g. Arndt and Christensen, 1992; Furman, 1995). The enriched geochemistry of many flood basalts suggests that these continental rifts are characterised by a plume-type source. Further evidence for a plume source is that the heat required for this style of magmatism could only be attributed to an upwelling mantle plume (e.g. Zhao et al , 1994; Storey et al., 1999; Rogers et al., 2000). A plume source for continental flood basalts is also supported by the notion that the onset of rifting is actively driven by the upwelling plume (e.g. Baker et al., 1996b; Garland et al., 1996; Spath et al., 2001).

(2) Enriched CLM: A number of studies have focussed on the role of a metasomatised continental lithospheric mantle (CLM) as a possible source for rift-related magmas (e.g. Hawkesworth, et al., 1992; Turner et al., 1996). Generally, melts generated from enriched CLM are characterised by an enriched incompatible element composition. This has been attributed to the incorporation of a rising plume and metasomatism by small volume, asthenosphere-derived melts (e.g. Paslick et al., 1995), or by subduction related enrichment (e.g. Oxburg and Parmentier, 1978; Menzies and Hawkesworth, 1987, Zhao and McCulloch, 1993a). Since melts passing through the crust can also experience enrichment (e.g. Rochell et al., 1995) there is considerable ambiguity whether slightly enriched compositions reflect

metasomatised CLM or crustal contamination (e.g. Glazner et al., 1991; Arndt et al., 1993). Many studies address both possibilities, and historically crustal contamination dominates the literature because of poor constraints on the highly variable composition of the CLM (McDonough, 1990; Glazner et al., 1991; Rochell et al., 1995).

(3) MORB: Continental rifts which have MORB-like chemical signatures are less common, except for most major oceans, and are generally not associated with well known continental rifts, such as the East African Rift (e.g. Fodor and Vetter, 1984; Wareham et al., 2001). MORB-like signatures have also been attributed to continental rifts associated with subduction related arc and back arc basins, with any trend towards enrichment accounted for by derivation from the continental lithosphere or subducted crust (e.g. Crawford and Berry, 1992; Curtis et al., 1999).

The purpose of this contribution is to investigate aspects of the geochemistry and isotopic signature of the mantle source region of the continental rift-related early Palaeozoic mafic dykes in the Harts Range region, in the eastern Arunta Block, central Australia. This study also contributes to the numerous studies of continental basalts, which attempt to clarify the origin of basalts in intracratonic settings (e.g. Cox and Hawkesworth, 1984; Hawkesworth et al., 1984; Hooper and Hawkesworth, 1993). In this paper, geochemical and isotopic data is presented on previously unrecognised, early Ordovician mafic rocks in central Australia, referred to here as the Harts Range Dykes. In combination with the metamorphic and structural framework that accompanies mafic magmatism, the geochemical and isotopic data provide insights into the evolution of the mantle reservoir beneath a newly recognised early Palaeozoic intracratonic rift in central Australia (Hand et al., 1999a; Mawby et al., 1999; Buick et al., 2001a,b).

2. Geological Framework

The Harts Range Dykes (HRD) constitute part of the highly deformed early Palaeozoic Harts Range Metamorphic Complex (Hand et al., 1999a; Mawby et al., 1999; Buick et al., 2001a), which forms part of the south-eastern Arunta Block (Fig. 1). Within the Harts Range Metamorphic Complex, two major lithological associations can be identified that define a cover and basement system (Fig. 1). The cover sequence is referred to here as the Irindina Supracrustal Assemblage, which was first interpreted as being deposited during the Palaeoproterozoic (ISA; Ding and James, 1985). This sequence was recently re-interpreted as having been deposited on a Palaeoproterozoic basement complex during mid-late Cambrian intracratonic rifting (Buick et al., 2001b) associated with the deposition of widespread marine sequences in the Amadeus and Georgina Basins (Fig. 1). This newly recognised rifting event appears to have been synchronous with widespread mafic magmatism along the eastern Australian continental margin (eg. Crawford and Keays, 1987; Turner and Foden, 1990; Turner, 1996; Foden et al., 2001), and was also approximately coeval with the extrusion of the continental Antrim Plateau flood basalts in north-western Australia (Hanley and Wingate, 2000) and the Table Hill basalts in southern Australia (Compston, 1974; Townson, 1985).

The Irindina Supracrustal Assemblage (Fig. 1) comprises a basal quartzite-calc-silicate association (Naringa Calcareous Member) which is overlain by a metapelitic-meta-igneous association (Irindina Gneiss and Harts Range Meta-Igneous Complex). The Harts Range Meta-Igneous Complex (Sivell and Foden, 1985) consists of a number of amphibolite bodies that parallel the tectonic layering, as well as plagioclase-rich (anorthositic) gneisses and ultramafic rocks. The geochemistry of the Harts Range Meta-Igneous Complex suggests it was generated in an intracratonic rift associated with a high degree of mantle partial melting at relatively low pressures (Sivell and Foden, 1985; Sivell, 1988). It is concluded later in this study, that the Harts Range Dykes, which are the focus of this investigation, are in part, genetically related to previously studied meta-tholeiites which constitute part of the Harts Range Meta-Igneous Complex (Sivell, 1988; Sivell and McCulloch, 1991). Together these rocks sample the uppermost depleted asthenosphere. The upper part of the Irindina Supracrustal assemblage consists of metapelites (Lower Brady Gneiss), overlain by calc-silicate units (Upper Brady Gneiss). Due to intense granulite to upper amphibolite-grade early Ordovician deformation (Hand et al., 1999a; Mawby et al., 1999; Buick et al., 2001a) the original thickness of the Irindina Supracrustal Assemblage is difficult to estimate. The present structural thickness is around 5-6 kilometres.

It has been previously accepted that the metasediments of the Harts Range Metamorphic Complex were deposited prior to 1750 Ma, based on U-Pb age dating of zircons from the Bruna Granite Gneiss (Cooper et al., 1988). However, recent age dating on

detrital zircons in metabasites and metapelites near Mallee Bore have yielded ages as young as 510 Ma (Buick et al., 2001a,b). This suggests that deposition of these sediments probably occurred during the early Palaeozoic rather than in the Palaeoproterozoic. The implications of those results for previous tectonic models will now require radical reconstruction (Buick et al., 2001b).

The Irindina Supracrustal Assemblage is in structural contact with an underlying Palaeoproterozoic basement complex comprising the 1745 Ma Bruna Granitic Gneiss (Cooper et al., 1988), and the underlying Entia Gneiss Complex, which are located within a regional domal structure; the Entia Dome (Fig. 1).

The Harts Range Metamorphic Complex underwent intense granulite to upper amphibolite grade early Ordovician metamorphism and associated intense deformation (Mawby et al., 1999; Hand et al., 1999a; Buick et al., 2001a). Peak metamorphic assemblages formed at around 825°C and 10.25 kbar (Miller et al., 1997; Mawby et al., 1999; Buick et al., 2001a) and were associated with extensive fluid-absent partial melting during the formation of a regional low-angle S1 gneissic layering. The peak assemblages have been overprinted by a system of extensional upper amphibolite-grade D2 fabrics that formed during approximately 10 kilometres of near-isothermal decompression of the terrain (Mawby et al., 1999) at around 470 Ma. Where the D2 fabrics have not been folded by later compressional structures, they vary from recumbent to moderately north-dipping and contain a well-developed north-northeast trending mineral lineation with top to the north shear sense indicators (Fig. 2).

2.1 The Harts Range Dykes

Although the mafic intrusives that are the focus of this study occur as both dykes and sills, they are referred to as the Harts Range Dykes (HRD) for convenience. In order to avoid potential confusion with older mafic rocks and structures in the Palaeoproterozoic basement to the Cambrian Irindina Supracrustal Assemblage (Buick et al., 2001b), this study focused exclusively on mafic intrusives found within the Irindina Supracrustal Assemblage, in order to be certain that they were Palaeozoic in age.

Within the Irindina Supracrustal Assemblage the Harts Range Dykes were emplaced syn-kinematically with the development of the early Ordovician retrograde D2 fabrics (Mawby et al., 1999). They are particularly voluminous within the regional-scale extensional detachment systems (Mawby, 2000) that lie north of Mt Ruby and Mt Palmer (Fig. 1), where they comprise between 5 and 20% of the outcrop (Fig. 3). Within these detachment systems the HRD are commonly associated with sills of garnet-bearing megacrystic granitic gneiss. Sill-like mafic bodies (40 x 60 metres) are approximately parallel to the S2 fabrics, but locally link to discordant dykes (Fig. 3) that vary in thickness between one and five metres. These

dykes can be traced for up to 60 metres until they are truncated by later gneissic fabrics interpreted to have formed during the latter stages of D2 (Mawby, 2000). The dykes typically trend E-W, however due to the intensity of D2 it is not clear if these orientations represent the primary emplacement orientation. Assuming that the orientation of the dykes reflects their original geometry, it suggests emplacement during approximate N-S extension, and is consistent with the N-S extension implied by the kinematics of the D2 fabrics (Fig. 2). Mawby et al., 1999; Mawby, 2000).

The majority of the dykes and sills are extensively recrystallised to variably foliated S2 assemblages, typically consisting of garnet-clinopyroxene-orthopyroxene-hornblende-plagioclase-quartz-ilmenite (Fig. 4a). P-T calculations from five garnet-bearing metamorphic assemblages suggest that recrystallisation occurred at 717 $\pm$ 27°C and 8.08 $\pm$ 0.79 kbars (2σ). Compositional data used in the P-T calculations is shown in Appendix A and B. These P-T conditions represent the intermediate early stages of the early Ordovician decompression of the terrain (Mawby et al., 1999). Although these recrystallised bodies locally truncate D2 fabrics, they are typically strongly deformed. These extensively recrystallised mafic intrusives contrast with some sills and dykes which show far less evidence of deformation and preserve relic igneous textures (Fig. 4b).

3. Analytical Procedures

The location of some of the analysed Harts Range Dyke samples is shown in Fig. 2. The locations of all the analysed dykes are documented in Appendix D.

Major and trace element analyses were determined by X-ray fluorescence techniques using the Philips PW 1480 100 kV X-ray fluorescence spectrometer, at Adelaide University. Major element analysis was carried out on fused glass discs of sample mixed with lithium meta/tetraborate flux (ratio sample:flux = 1:4). Trace elements were analysed on pressed pellets.

REE abundances were determined using the Thermo Optek Plasma Quad 3 (ICP-MS) by Amdel Limited, Adelaide. The solution for analysis was prepared using a normal 'whole rock' method in which a sub-sample was fused at 1000^{o}C with a borate flux. The resultant glass was then leached with an acid solution to give a total solution of the sample. This solution was then diluted x10 in order to add an internal standard for instrumental drift correction and read on the ICPMS against calibration standards in a similar matrix. The error for this method is quoted as + 3% relative for the major components.

Nd and Sr isotope compositions were determined using isotope dilution methods on a Finnigan MAT 262 thermal ionisation mass spectrometer and Sm isotope analysis using a Finnigan MAT 261 thermal ionisation mass spectrometer in static mode, at Adelaide University. Analytical procedures are given by Foden et al., (1995) and Foden et al., (2001). The long-term reproducibility of the complete analytical procedure is measured by the analysis of an in-house standard; the standard deviation is 8 ppm for $^{87}Sr/^{86}Sr$ and 13 ppm for $^{143}Nd/^{144}Nd$. Sm- and Nd-concentrations were determined by isotope dilution following aliquoting and spiking. Machine performance is monitored by the analyses of international standards. Over the course of this study we returned $^{143}Nd/^{144}Nd$ values for the La Jolla standard of 0.511860 ± 7 (n = 13).

4. Geochemical Results

4.1 Major element chemistry

Major element whole rock concentrations for analysed samples from the Harts Range Dykes are presented in Tables 1 and 2. The HRD are sodic ($Na_2O > K_2O$) meta-tholeiitics which have variable SiO_2 contents within the basalt range (44.35 - 52.21 wt%) and exhibit high Al_2O_3 concentrations (10.83-17.53 wt%) with variable P_2O_5 (0.04-0.38 wt%) and TiO_2 (0.67-2.88 wt%). The wide range of MgO (5.61 – 14.14 wt%) concentrations that decrease with increasing Zr content indicate that crystal fractionation processes play a significant role in the chemical variation of these rocks (e.g. Sivell, 1988). The HRD cover a considerable range in Mg# [100 x Mg^{2+} / (Mg^{2+} + ΣFe)] from 34.40 – 70.00 (average 55.60) and show varying degrees of correlation in major element diagrams (Fig. 5). There is an increase in Al_2O_3 with increasing Mg#, which is linked to fractionation processes. Other significant trends that are indicative of fractionation processes are the increase of TiO_2 and Fe_2O_3T and decrease of MgO with declining Mg# (Fig. 5).

4.2 Trace element and isotopic chemistry

Based on trace element and isotopic criteria the HRD dykes can be subdivided into two suites. For the purposes of this investigation they will be referred to as the Group 1 dykes and the Group 2 dykes.

Whole rock trace element data from both groups of dykes are shown in Tables 1 and 2. Based on Zr versus Nb (Fig. 6), two distinct fractionation trends exist. This data correlates well with the Pearce Element Ratio (PER) plot (Fig. 6), which shows that the HRD contain two separate cogenetic suites (e.g. Stanley and Russell, 1989). There are obvious differences in ratios such as Th/Zr (avg. Group 1 = 0.02 and avg. Group 2 = 0.03), Th/Nb (1.0 and 0.4) and Zr/Nb (62 and 14) (Fig. 7). These ratios are useful because they are known to be less affected by melting in the source region or by magmatic processes and thus the differences in these ratios exhibited by the dykes suggest the two groups are not genetically related (Ayuso et al., 1998).

Trends that are common to both suites of dykes are the decrease of Cr with declining Mg# and the increase of Zr with declining Mg# (Fig. 7), which are indicative of fractionation processes (Spath et al., 2001).

Group 1 dykes are characterised by higher Zr and Y but lower Nb, Ba, La and Ce contents on Mg# diagrams. These dykes show characteristics such as high Mg# and high Ni (average = 92 ppm), Cr (303 ppm) and Co (63 ppm) that are indicative of primary basalts (e.g. Ayuso et al., 1998). Conversely, the Group 2 dykes have lower Zr and Y contents, but

have higher Nb, Ba, La and Ce contents. The Group 2 dykes have similar Mg# and Co (66 ppm) but higher Ni (172 ppm) and Cr (530 ppm) values than the Group 1 dykes, but are still consistent with primary basaltic melts (e.g. Ayuso et al., 1998).

Chondrite normalised rare-earth patterns of 14 representative samples are illustrated in Fig. 8. The Group 1 dykes have a flat REE pattern with $(La/Yb)_N$ = 1.21 and depleted $(La/Sm)_N$ values of 0.70. Conversely, the Group 2 dykes have steeper patterns with $(La/Yb)_N$ = 5.12 with fractionated $(La/Sm)_N$ values of 1.90. Both groups have near-absent Eu*/Eu anomalies. The sub-parallel, REE patterns suggest that melt compositions have been modified by variables other than fractional crystallisation (Schmitz et al., 1995). On the MORB-normalised incompatible trace element plot (Fig. 8D) the pattern of the Group 2 dykes parallels a pattern exhibited by island arc tholeiites with slightly higher element abundances (Pearce, 1983).

Sr and Nd-Sm isotopic compositions for five representative whole-rock samples are listed in Table 3. $\varepsilon_{Nd}(480)$ values for the Group 1 dykes are +5.3 and +6.7, with higher $^{143}Nd/^{144}Nd$ (0.512260-0.512328), but lower $^{87}Sr/^{86}Sr$ (0.703281-0.703568) values. The Group 2 dykes have highly variable negative $\varepsilon_{Nd}(480)$ values which range from –11.5 to –0.04 and have lower $^{143}Nd/^{144}Nd$ (0.511856 - 0.512528) values and higher $^{87}Sr/^{86}Sr$ (0.704931 - 0.722709) values. A plot of ε_{Nd} versus time is illustrated in Fig. 9.

5. Interpretation of Compositional Data

5.1 Element mobility

An inevitable consequent of studying recrystallised igneous rocks is the unknown modifications to rock compositions imposed by metamorphism (eg. Sivell et al., 1985; Amelin and Semenov, 1996). This problem is especially relevant in the case of the Palaeozoic Harts Range Dyke suite, which have been affected by granulite to upper amphibolite facies metamorphism. The assessment of igneous fractionation processes that transpired before metamorphism is dependent on the degree to which metamorphism was isochemical (eg. Sivell et al., 1985). The HRD exhibit good linear correlation of Zr with various incompatible elements, such as Ti and Y. These elements are generally thought to be immobile during most metamorphic conditions (e.g. Weaver and Tarney, 1981; Sivell and Foden, 1985) and most likely reflect original igneous fractionation processes for the meta-basaltic dykes (Fig. 10). Preferential trace element mobility and redistribution by metamorphism are responsible for poor correlation of some LIL-elements such as K, Sr and Ba. Hence, the analysis of the HRD using LIL-elements should be treated with care. Previous work concerning REE distribution patterns suggest that REEs probably remain immobile during amphibolite-granulite facies metamorphism (e.g. Hamilton et al., 1979; Hajash, 1984; Bartley, 1986) and moderately regular observed REE distributions most likely reflect original igneous patterns. Relatively sub-parallel REE patterns indicate that fractionation of REE during metamorphism has not been severe. Based on these inferences, the effect of metamorphism and other secondary alteration processes on the chemistry of the dykes has been negligible.

5.2 Investigations of the tectonic setting

Although the tectonic setting associated with the emplacement of the Harts Range Dykes is known to be an intracratonic rift (Hand et al., 1999a; Mawby et al., 1999; Buick et al., 2001a), tectonic discrimination diagrams imply a variety of tectonic settings. This indicates that basalt geochemistry may not be always be a true reflection of tectonic setting associated with melting, but rather, an indication of the type of mantle source and processes that provide melts (e.g. Zhao and McCulloch, 1993a).

Zr-Nb-Y variation (Fig. 11; Meschede, 1986), classifies the Group 1 dykes in the field of N-type MORB and volcanic arc basalts. The Group 2 dykes lie in several fields with either an enriched MORB and volcanic arc composition. MnO-TiO_2-P_2O_5 variation (Fig. 12; Mullen, 1983), suggest that magma generation for Group 1 dykes occurred in a MORB-type setting but Group 2 dykes originated from an island arc type source.

Trace and major element discrimination criteria suggest that the Group 1 dykes have N-type MORB affinities which is consistent with other geochemical and isotopic data (see below). The Group 2 dykes have an enriched signature which could be attributed to subducted material associated with volcanic or island arcs (e.g. Wittke et al., 1989; Zhao and McCulloch, 1993a).

5.3 The effects of fractional crystallisation

Analysing systematic variations of incompatible element concentrations can identify the processes that control magma genesis (eg. Sivell and Foden, 1985). Ti, Zr and Y are especially useful, for the identification of minerals likely to be controlling geochemical evolution, due to their relative immobility during metamorphism of basaltic rocks and hence are a reflection of original igneous processes (Pearce and Cann, 1973). TiO_2 and Y contents of the HRD are strongly correlated (Fig. 10) and their abundance levels increase with decreasing Mg#. These straight-line trends through the origin on biaxial plots (incompatible versus slightly incompatible trace elements) are consistent with series related by crystal fractionation (eg. Treuil and Varet, 1973; Sivell and Foden, 1985). The HRD have TiO_2 and Y contents which fall along a fractionation trend corresponding to that exhibited by N-type MORB. This kind of variation could be explained by a model suggesting that plagioclase and/or olivine and clinopyroxene are the dominant fractionating minerals (Sivell and Foden, 1985). The precipitation of hornblende or magnetite, which strongly fractionate Ti from Y (Sivell and Foden, 1985), would lead to lower Ti/Y ratios in derivative liquids than in the original liquids, and are considered not to have been significant fractionating phases. The presence of hornblende in some samples is probably metamorphic in origin.

The trends observed in oxide and trace element data versus Mg# (Fig. 5 and 7), especially Zr, imply that much of the chemical variation in the HRD may be attributed to fractional crystallisation (Sivell and Foden, 1985; Sivell, 1988; Spath et al., 2001). In Fig. 5, the increase of Al_2O_3 with increasing Mg# suggests that clinopyroxene ± olivine crystallised without plagioclase. This is further supported by Fig. 7, which shows a decrease in Cr with declining Mg#. A positive trend between Ni (max 382 ppm) and Mg# suggests that olivine was also an important fractionating phase. The removal of Zr and TiO_2 from magmas during the fractionation of olivine, pyroxene and plagioclase causes the negative trends seen in Fig. 7, implying that these minerals formed in the melt. In basaltic melts, the Mg/Fe ratio usually falls steadily through each stage of crystallisation, since common ferro-magnesium minerals have higher Mg/Fe ratios than the liquids from which they fractionated (Cox et al., 1979). The negative correlation of Fe_2O_3T and positive correlation of MgO with Mg# (Fig. 5), suggests that the fractionation of olivine would have been dominant.

In general terms, the major element variation is consistent with an evolutionary path dominated by olivine fractionation and to a lesser extent clinopyroxene and plagioclase fractionation. This observation is consistent with fractional crystallisation of modern MORB in which the crystallisation order is olivine, plagioclase and clinopyroxene (Green et al., 1979; BVSP, 1981).

5.4 Implications of isotopic data

The isotopic data define two compositional groups with one suite occupying the positive ε_{Nd} field, and the other suite characterised by a broad negative ε_{Nd} field (Fig. 9). This distinction is consistent with the groupings defined by trace element geochemistry and REE patterns. The large variation in $\varepsilon_{Nd}(480)$ values for the whole rocks (-11.5 to +6.7) suggests variable amounts of crustal contamination of the magma source (e.g. Pinese et al., 1995) and could be the result of multiple magma injections with differing degrees of contamination (e.g. Amelin and Semenov, 1996).

Fractional crystallisation or partial melting in the source region cannot explain isotopic variations, because these processes do not affect such ratios (e.g. Ayuso et al., 1998). The broadly heterogeneous isotopic compositions of the HRD exclude an evolution by any closed-system fractionation process. However, the presence of a single curve observed between $\varepsilon_{Nd}(480)$ and $(^{87}Sr/^{86}Sr)_i$ suggest that simple two component mixing or assimilation and fractional crystallisation processes may exist (DePaolo, 1981).

The highest initial $\varepsilon_{Nd}(480)$ values observed in the HRD come from the Group 1 dykes (+6.7 and +5.3). These values are close to those predicted for the depleted mantle and thus show little evidence for crustal contamination. It is proposed that the Group 1 dykes isotopic values would be a good estimate for the composition of the asthenospheric mantle beneath the Larapinta rift at around 480 Ma. The Group 1 dykes have similar isotopic values to meta-tholeiites of the Harts Range Meta-igneous Complex (Sivell and McCulloch, 1991; Fig. 9). However, the ε_{Nd} values of the meta-tholeiites were calculated assuming an age of 1750 Ma (Sivell and McCulloch, 1991), and were interpreted as originating from an ultra-depleted mantle source. When an early Palaeozoic age is used, the calculated $\varepsilon_{Nd}(480)$ values plot close to the depleted mantle array. The near exactness of the ε_{Nd} values of meta-tholeiites belonging to the Harts Range Meta-Igneous Complex and Group 1 dykes, suggests both belong to the same suite. Furthermore, the major and trace element data indicate these two suites of rocks are genetically related (Figs. 5 and 7). In contrast, the Group 2 dykes geochemically appear to be a different suite of rocks.

Three samples representative of the Group 2 dykes are characterised by negative $\varepsilon_{Nd}(480)$ values of -11.5, -2.1 and –0.04. These enriched compositions may suggest varying

degrees of crustal contamination of a mantle source (e.g. Hawkesworth et al., 1984; Rochell et al., 1995), in which case, the original mantle source chemistry cannot be determined. Alternatively, the average negative $\varepsilon_{Nd}(480)$ values for the Group 2 dykes may possibly suggest derivation from an old and enriched continental lithosphere (e.g. Wittke et al., 1989; Zhao and McCulloch, 1993a; Cousens et al., 2001; see below).

6. Discussion

6.1 Mantle source heterogeneity

The question of whether a suite of basalts has been contaminated by continental crust is critical to the evaluation of their source characteristics. The problem is particularly evident in cases where an enriched signature is observed, since derivation from enriched mantle sources and assimilation of continental crust may yield similar compositional characteristics (Rocholl et al., 1995).

The elevated Zr/Nb ratio (avg. 62) and low Ba/Zr (avg. 0.5) exhibited by the Group 1 dykes suggests a more depleted, heterogenous mantle source than that of the Group 2 dykes (e.g. Erlank and Kable, 1976; Sivell and Foden, 1988). This is supported by the chondrite normalised REE pattern of the Group 1 dykes, which is similar to that observed by an N-type, depleted, MORB source. Furthermore, their limited range of isotopic values lie close to pure N-type MORB depleted mantle values. Data from the mid-late Cambrian Harts Range meta-tholeiites (Sivell, 1988; Sivell and McCulloch, 1991) and amphibolites (Sivell and Foden, 1985) have also suggested that derivation from upper mantle MORB-like sources was most likely. The geochemistry of those rocks is consistent with a high degree of mantle partial melting at low pressures in an intracratonic rift setting.

Conversely, the Group 2 dykes are interpreted as being derived from a slightly enriched mantle source with possible various sources of enrichment evaluated below. The Group 2 dykes have intermediate average values for Zr/Nb of 14 and Ba/Zr of 2.6, consistent with an arc-like, but isotopically variable mantle source (Saunders et al., 1980; Sivell, 1988).

The HRD do not exhibit a pure, enriched and ideal plume-type signature such as the basalts from the East African rift (Rogers et al., 2000), and it is unlikely that a major upwelling mantle plume was responsible for the slightly enriched chemical signatures of the Group 2 dykes.

6.2 The nature of enrichment: crustal contamination or an ancient continental lithospheric mantle source?

The enriched chemical signature exhibited by the Group 2 dykes is indicative of a number of sources or processes. These are addressed in detail below:

6.2.1 Crustal Contamination

The broadly heterogeneous isotopic compositions from the HRD appear to preclude an evolution by any closed-system fractionation process (e.g. Amelin and Semenov, 1996). One

of the most important open-system processes that could account for the geochemical features of the Harts Range Dykes is crustal contamination (e.g. Sherton et al., 1990; Wirth and Vervoort, 1995; Ayuso et al., 1998). Crustal contamination in its simplest terms, and as applied here, is the contamination of magmas by crustal material as they migrate up through the continental crust (e.g. Hawkesworth et al., 1984; Hansen and Nielsen, 1999). This assessment does not attempt to recognise the chemical effects of relict crustal components in the upper mantle (White and Hofmann, 1982). The debate between crustal contamination versus enriched mantle as the primary control on the composition of LREE mafic melts will only be settled when the nature of the geochemical extent of mantle enrichment is fully defined by the analysis of mantle xenoliths (Hawkesworth et al., 1984; McDonough, 1990).

Correlations observed between isotope ratios and the inverse of the corresponding elemental concentrations are also valuable in assessing the role of crustal contamination, although linear trends on these diagrams can also reflect mechanical mixing of magma sources (Hansen and Nielsen, 1999; Rogers et al., 2000). The broadly positive linear trend for the Group 2 dykes observed in Fig. 13A, argues strongly for crustal contamination or mixing of magma sources. The positive SiO_2 and Sr-isotope correlation (Fig. 13B) and their wide variation suggest the melts were subject to crustal contamination, and may have experienced an assimilation and fractional crystallisation process (DePaolo, 1981).

The LREE enriched nature and negative initial ε_{Nd} values for the Group 2 dyke samples is a clear indication that there is a component with a long term history of LREE enrichment and a Sm/Nd ratio significantly less than chondrite in those dykes. Elevated SiO_2 contents, high initial Sr-isotope ratios and lowered Nb contents relative to La, Ce, K and Th, are commonly used as an indication for felsic crustal contamination (Larsen et al., 1989; Hansen and Nielsen, 1999). However, these inferences dominate the literature because of the notion that felsic crustal rocks are potentially the most fusible crustal components (Glazner et al., 1991; Thompson et al., 1993).

In order to asses the relative roles of mantle and crust in the petrogenesis of the HRD the compositions of the dykes have been examined in relation to the estimated compositions of melts derived from the depleted mantle (N-type MORB) and various crustal sources at 480 Ma. Isotopic data from the Bruna Granite (Entia Dome: Foden et al., 1995) and quartzofeldspathic calc-silicate rocks (SMC: Windrim and McCulloch, 1986) that from the basement to the Irindina Supracrustal Assemblage (James and Ding, 1988; Hand et al., 1999b), were used in separate simple two-component mixing models (Fig. 14). The presence of a broad single curve linking ε_{Nd} and Sr allows for simple mixing modelling (DePaolo, 1981).

Using an age of 480 Ma, all five dyke samples closely fit the mixing curve, which uses the Bruna Granite as the contaminant (Fig. 14). Fig. 14 illustrates that the two Group 1 samples can be modelled by adding a negligible amount of crust to average N-type MORB. Group 2 dykes require 6%, 8% and 23% of crust to explain their isotopic composition. This

modelling indicates that the Group 1 dykes would have experienced minor contamination, whereas varying amounts of crust contaminated the Group 2 melts. While the results of this modelling appears to fit the isotopic data well, they are not consistent with the SiO_2 contents (Fig. 13) and basaltic nature of the three representative Group 2 dyke samples. Assimilation of an Eu-depleted crust can be ruled out because of the absence of a significant Eu anomaly in the REE patterns (Storey et al., 1999).

While it is widely accepted that a felsic source is more fusible than a dry mafic rock (e.g. Hergt et al., 1991; Thompson et al., 1993), a hydrated crustal mafic rock is a potential candidate for partial melting (Peng et al., 1994). Historically, contamination of melts by silicic crust is often assumed, however, it makes sense to model mafic contaminants because they dominate the lower crust (e.g. Fountain and Salisbury, 1981). A study by Peng et al., (1994) on formations of the Deccan Traps suggests a model in which crustal contamination by amphibolites yields extremely negative ε_{Nd} values (-20). Gabbro, metasomatised by a water rich fluid would yield an amphibolite capable of anatexis, via generalised melting reactions such as:

(1) Hbd + Plag + Qtz → Cpx + Ca-rich Plag + Melt ± Ilm
(Rushmer, 1991)

(2) Hbd + Plag → Liquid + Cpx + Al-rich Hbd + Ca-rich Hbd + Opx + Gt
(Wolf and Wyllie, 1994)

In the case of reaction (1), the resulting melt would have a tonalitic composition and in reaction (2) the melt would have a high-Ti basaltic to high-Al tonalitic composition.

The isotopic signatures observed for the Group 2 dykes could only be achieved if the crustal component was significantly old and had an enriched isotopic ratio, or was metasomatised by an isotopically enriched fluid (e.g. Peng et al., 1994). In reference to the HRD, a possible source of mafic crustal contamination could be amphibolites from Palaeoproterozoic Entia Gneiss Complex (EGC), which forms basement to the Irindina Supracrustal Assemblage. Meta-basic rocks in the EGC have trace element compositions which typify subduction-related magmas (Foden et al., 1995), as do the Group 2 dykes (Fig. 8). The ε_{Nd} values of the amphibolites correspond with the values of the Group 2 dykes at 480 Ma, however, this implies that almost 100 percent of the contaminant would be required to achieve values of the Group 2 dykes (Fig. 9). If this were the case the dykes should exhibit a tonalitic-like composition according to reactions 1 and 2. Furthermore, the Sr-isotope ratios of the amphibolites are not high enough to allow for successful mixing modelling with the Group 2 dykes.

6.2.2 Continental lithospheric mantle

In contrast to the crustal assimilation model, a number of geochemists favour enriched mafic magma generation of continental basalts within a metasomatised continental lithosophere mantle (CLM; e.g. Hergt et al., 1991; Brandon and Goles, 1995; Cousens et al., 2001). Using spinel-bearing xenoliths, McDonough (1990) assessed the composition of the CLM and concluded that the reservoir has an incompatible trace element enriched character that varies in composition and in age (see also, Hawkesworth et al., 1992). The values of Rb, Ba, Th and Nb and Zr discussed and postulated for the CLM by McDonough (1990) are much lower than those of the Group 2 dykes (Table 5). Additionally, the composition of the CLM (McDonough, 1990) does not show the same LIL-element enriched and HFS-element depleted signature as the Group 2 dykes (Table 5). Many studies, which suggest a CLM source, have highly negative ε_{Nd} values (ε_{Nd} = -10, Hawkesworth et al., 1984; Farmer et al., 1989; Cousens et al., 2001) that imply isotopic isolation from the underlying, convecting asthenospheric mantle for hundreds of millions of years (e.g. Hawkesworth et al., 1984; Hawkesworth et al., 1992; Cousens et al., 2001). However, these highly negative ε_{Nd} values may not necessarily be a characteristic of all CLM, since some authors have defined this source region with rocks exhibiting low, positive values (e.g. Brandon and Goles, 1995).

The composition of the CLM is difficult to constrain for local regions because of its highly variable composition over small-scales distances (McDonough, 1990; Hawkesworth et al., 1992). This variability is highlighted by a comparison of key data in Table 5, which compares data from this study, with that of subduction-modified CLM and unmodified CLM. This variability in degree of enrichment is due to a number of different enrichment processes and sources, including the passive incorporation of the asthenosphere onto the base of the lithosphere as it cools, and diapiric underplating (McDonough, 1990; Hawkesworth et al., 1992). This compositional variability makes it difficult to compare the central Australian CLM with other known provinces, such as beneath the western U.S. (e.g. Brandon and Goles, 1995). Therefore, it would be best to compare the unknown enriched suite of rocks (Group 2 dykes) with a suite of rocks of close proximity, which has been interpreted as a derivative of the CLM (see next section).

6.2.3 Subduction-modified continental lithospheric mantle

The central Australian crust has been intruded by a number of suites of mafic rocks that vary in age from 1800 – 480 Ma (e.g. Sivell, 1988; Sivell and Foden, 1988; Zhao and McCulloch, 1993a). The late Proterozoic Stuart Dyke Swarm (~1080 Ma; Zhao and McCulloch, 1993b) is an example of one such suite and is used here to compare its enriched composition with that of the Group 2 dykes. These dykes dominantly trend N-S and intrude

the Southern Province of the Arunta Block. Spatially, the dykes are further than 200 kilometres to the west of the Harts Range (Zhao et al., 1994), but unclassified N-S trending dykes occur less than 50 kilometres to the west of the Harts Range. On the basis of geochemical data, these dykes were interpreted as being derived by partial melting of the continental lithospheric mantle which was created from a portion of the mantle, metasomatised by slab-derived components during subduction. This metasomatised domain later became isolated from the convecting asthenosphere. (Zhao and McCulloch, 1993a).

Table 5 illustrates the elements and ratios that reflect LIL-element enrichment and HFS-element depletion consistent with material from a subducted slab. The values for the Group 2 dykes and the Stuart Dyke Swarm (SDS) are similar. Another study (Wittke et al., 1989), which identifies a CLM metasomatised by subducted fluids, is also compared in Table 5. The compositions indicate that the nature and degree of enrichment by a subducting slab is widely variable and may be dependent on fluid dynamics and the nature of the slab. The closeness of fit of the Group 2 dykes and the SDS is also evident in the chondrite normalised REE pattern and MORB normalised incompatible trace element pattern (Fig. 8). The Group 2 dykes, like the SDS, have a trace element pattern consistent with derivation from a magma source similar to that of island-arc tholeiites (Pearce, 1983). This interpretation fits well with the tectonic discrimination diagrams based on major and trace element variation (Fig. 11 and 12). Zhao and McCulloch (1993a) attribute the variable and highly negative ε_{Nd} values for the SDS to a subduction-modified CLM, which had been isolated for several hundred million years prior to partial melting. The ε_{Nd} values for the Group 2 dykes fall within the values of the SDS at 480 Ma (Fig. 9), suggesting derivation from a similarly composed CLM to that which generated the SDS.

6.3 Sources of early Palaeozoic mafic magmatism in the eastern Arunta Block

Assessment of the Group 2 Harts Range Dykes in comparison to a crustal contamination model and a variety of CLM sources suggest that a subduction-modified CLM is the most likely reservoir for this dyke suite. Due to the variability of the CLM, its bulk average composition may not be a clear indication of whether or not it could be a possible source for the Group 2 dykes. Given the argument for the subduction-modified CLM, it is concluded that the average bulk CLM is not likely to be a significant contributor to the chemical signature of the Group 2 dykes in the Harts Range, because it does not exhibit a HFS-element depleted and LIL-element enriched signature. It is equally likely that mafic crustal contamination and a subduction-modified CLM is responsible for the geochemical and isotopic characteristics exhibited by the Group 2 dykes. Although mafic crustal contamination is a plausible concept, it is ruled out as a major source of enrichment because of the inability to match the isotopic data of a likely contaminant (basement amphibolites) with that of the

Group 2 dykes. It could be envisaged that both Group 1 and 2 dykes were derived from the same source, and that the Group 2 dykes had experienced variable amounts of crustal contamination. The simple geochemical comparison between data from the Stuart Dyke Swarm (1080 Ma) and the Group 2 Harts Range Dykes suggest the two suites were derived from a similar CLM. This CLM has been metasomatised by fluids and material from the subducted slab (Zhao and McCulloch, 1993a) and up until, at least 480 Ma, has remained compositionally intact and isolated from the underlying convecting asthenosphere.

The question that now remains is to explain the coexistence of both N-type MORB dykes (Group 1) and subduction-modified CLM dykes (Group 2), in time and space. Figure 15 is a schematic model which attempts to describe a likely scenario for the emplacement of both groups of the HRD. It shows that a depleted mantle wedge was metasomatised by a subducting slab and associated fluids during the Proterozoic (c. 1760-1750 Ma) around which time Cordilleran-style batholiths were emplaced (Cooper et al., 1988; Foden et al., 1988). The resulting enriched mantle was isolated from the underlying convecting mantle up until the late Proterozoic. The partial melting of the CLM at around 1080 Ma resulted in the emplacement of the Stuart Dyke Swarm (Zhao and McCulloch, 1993a), however, the causes of melting at this time are unknown. Continued isotopic isolation persisted up until the late Cambrian when the onset of N-S extensional rifting occurred (Hand et al, 1999a; Mawby et al., 1999; Buick et al., 2001a,b). At this time the lithosphere in the eastern Arunta Block attenuated leading to decompressional melting of the depleted mantle. The resulting melts advected heat into the overlying CLM, which inturn underwent partial melting. Dykes and sills of both the depleted mantle and subduction-modified CLM were emplaced syn-kinematically into the Harts Range Metamorphic Complex as it underwent decompression linked to ongoing early Ordovician extension. The early Palaeozoic N-S extension in central Australia created a dextral pull-apart basin, similar to a number of basins associated with lithospheric extension of the Rio Grande Rift (e.g. Aldrich and Dethier, 1990). These basins, like that associated with the early Palaeozoic extension in central Australia, also contain mafic magmas emplaced as a result of decompressional melting of the mantle (Thompson and Gibson, 1994).

7. Conclusions

The early Ordovician (c. 480 Ma) Harts Range mafic dykes were emplaced into the mid-late Cambrian Irindina Supracrustal Assemblage, central Australia, and are the mafic igneous expression of early Palaeozoic intracratonic extension. The dykes are preferentially located within regional-scale ductile detachments and were emplaced and deformed at temperatures of around 700^{o}C and at depth of approximately 30 kilometres, during N-S extension. Two different sources account for the chemical diversity observed in the HRD and define two distinct magmatic suites. Geochemical and isotopic data from the HRD suggests the following:

1. Major element data does not distinguish between the two suites but trends, common to both groups, can be accounted for by the fractional crystallisation of olivine, pyroxene and plagioclase. Group 1 dykes exhibit higher concentrations of Zr and Y but lower Nb, Ba, La and Ce relative to those of the Group 2 dykes. This distinction also matches well with the REE data with the Group 1 dykes having an N-type MORB patterns and the Group 2 dykes having a separate E-type MORB pattern.
2. The Group 1 dykes have a composition similar to that of N-type MORB and their positive ε_{Nd} values represent minimum values for the upper depleted asthenosphere at 480 Ma. The Group 2 dykes reflect an E-type MORB composition, which is the result of partial melting of a subduction-modified continental lithospheric mantle, similar to that resulting in the Stuart Dyke Swarm at 1080 Ma. The highly enriched isotopic characteristics can be attributed to the isolation of this reservoir from the convecting asthenosphere for hundreds millions of years.
3. Enrichment of the Group 2 dykes by crustal contamination is considered, but a felsic component is eliminated because the basaltic nature cannot account for the amount of crust required to fit the isotopic data. Conversely, mafic crustal contamination is suggested to be a plausible contaminant, but is not favoured because likely contaminants do not fit the isotopic data of the Group 2 dykes. Furthermore, the bulk average continental lithospheric mantle is rejected as a source for the Group 2 dykes, because its composition should be enriched in incompatible elements, and not reflect LIL-element enrichment and HFS-element depletion like the Group 2 dykes.
4. Early Palaeozoic N-S extension led to decompressional melting of the upper depleted asthenospheric mantle causing magma ascent and advected heating of the overlying CLM. Together the partial melts were emplaced syn-kinematically into the Harts Range Metamorphic Complex, creating two geochemically distinct suites of dykes.

Reference

Aldrich, M.J.Jr., Dethier, D.P., 1990. Stratigraphic and tectonic evolution of the northern Espanola Basin, Rio Grande Rift, New Mexico. Geo. Soc. America. Bull. 102, 1695-1705.

Amelin, Y.V., Semenov, V.S., 1996. Nd and Sr isotopic geochemistry of mafic layered intrusions in the eastern Baltic shield: implications for the evolution of Paleoproterozoic continental mafic magmas. Contrib. Mineral. Petrol. 124, 255-272.

Arndt, N.T., Christensen, U., 1992. The role of lithospheric mantle in continental flood volcanism: thermal and geochemical constraints. J. Geophysical Res. 97, 10967-10981.

Arndt, N.T., Czamanske, J.L., Wooden, J.L., Federenko, V.A., 1993. Mantle and crustal contributions to continental flood volcanism. Tectonophysics 223, 39-52.

Ayuso, R.A., De Vivo, B., Rolandi, G., Seal II, R.R., Paone, A., 1998. Geochemical and isotopic (Nd-Pb-Sr-O) variations bearing on the genesis of volcanic rocks from Vesuvius, Italy. J. Volcanology. Geothermal Res. 82, 53-78.

Baker, J.A., Thirlwall, M.F., Menzies, M.A., 1996a. Sr-Nd-Pb isotopic and trace element evidence for crustal contamination of plume-derived flood basalts: Oligocene flood volcanism in western Yemen. Geochim. Cosmochim. Acta. 60 (14), 2559-2581.

Baker, J.A., Snee, L. W., Menzies, M.A, 1996b. A brief Oligocene period of flood volcanism in Yemen; implications for the duration and rate of continental flood volcanism at the Afro-Arabian triple junction. Earth Planet. Sci. Lett. 138, 39-55.

Baldridge, W.S., Perry, F.V., Vaniman, D.T., Nealey, L.D., Laughlin, A.W., Kyle, P., Bartov, Y., Steinitz, G., Gladney, E.S., 1991. Middle to late Cenozoic magmatism of the southeastern Colorado Plateau and central Rio Grande rift (New Mexico and Arizona, U.S.A.): a model for continental rifting. Tectonophysics, 197, 327-354.

Bartley, J.M., 1986. Evaluation of REE mobility in low-grade metabaslats using mass – balance calculations. Norsk Geol. Tidssk, 66, 145-152.

Brandon, A.D., Goles, G.G., 1995. Assessing subcontinental lithospheric mantle sources for basalts: Neogene volcanism in the Pacific Northwest, USA as a test case. Contrib. Mineral. Petrol. 121, 364-379.

Buick, I.S., Miller, J.A., William, I.S., Cartwright, I., 2001a. Ordovician high-grade metamorphism of a newly recognised late Neoproterozoic terrane in the northern Harts Range, central Australia. J. Metamorphic Geol. 19, 373-394.

Buick, I.S., Miller, J.A., Williams, I.S., Hand. M., Mawby, J., 2001b. Deep holes in the Centralian Superbasin, SHRIMP zircon constraints on the depositional age of granulites in the eastern Arunta Block. Geol. Soc. Aust. Abstracts, SGTSG, 64, 13-14.

BVSP (Basaltic Volcanism Study Project), 1981. Basaltic Volcanism on the Terrestrial Planets. Pergamon, New York, N.Y., pp. 1286.

Compston, W., 1974. The Table Hill Volcanics of the Officer Basin, Precambrian or Paleozoic? J. Geol. Soc. Aust. 21, 403-411.

Cooper, J.A., Mortimer, G.E., James, P.R., 1988. Rate of Arunta Inlier evolution at the eastern margin of the Entia Dome, central Australia. Precambrian Res. 40/41, 251-276.

Cousens, B.L., Aspler, L.B., Chiarenzelli, J.R., Donaldson, J.A., Sandeman, H., Peterson, T.D., LeCheminant, A.N., 2001. Enriched Archean lithospheric mantle beneath western Churchill Province tapped during Paleoproteozoic orogenesis. Geol. 29, 827-830.

Cox, K.G., Bell, J.D., Pankhurst R.J., 1979. The Interpretation of Igneous Rocks. London, George Allen and Unwin. pp 450.

Cox, K.G., Hawkesworth, C.J., 1984. Relative contributions of crust and mantle to flood basalt magmatism, Mahabaleshwar area, Deccan Traps. Philos. Trans. R. Soc. London. Ser. A. 310, 627-641.

Crawford, A.J. Keays, R.R., 1987. Petrogenesis of Victorian Cambrian tholeiites and implications for origin of associated boninites. J. Petrol. 28, 1075-1109.

Crawford, A.J., Berry, R.F., 1992. Tectonic implications of Late Proterozoic – Early Palaeozoic igneous rocks associations in western Tasmania. Tectonophysics, 214, 37-56.

Curtis, M.L., Leat, P.T., Riley, T.R., Storey, B.C., Millar, I.L., Randall, D.E., 1999. Middle Cambrian rift-related volcanism in the Ellsworth Mountains, Antarctica; tectonic implications for the palaeo-Pacific margin of Gondwana. Tectonophysics, 304, 275-299.

DePaolo, D.J., 1981. Trace element and isotopic effects of combined wallrock assimilation and fractional crystallisation. Earth Planet. Sci. Lett. 53, 189-202.

Ding, P. James, P.R., 1985. Structural evolution of the Harts Range area and its implications for the development of the Arunta Block, Central Australia. Precambrian Res. 27, 251-276.

Erlank, AJ., Kable, E.J.D., 1976. The significance of incompatible elements in Mid-Atlantic Ridge basalts from 45ºN, with particular reference to Zr/Nb. Contrib. Mineral. Petrol. 54, 281-291.

Farmer, G.L., Perry, F.V., Semken, S., Crowe, B., Curtis, D., DePaolo, D.J., 1989. Isotopic evidence on the structure and origin of subcontinental lithospheric mantle in Southern Nevada. Journal of Geophysical Res. 94, 7885-7898.

Foden, J.D, Buick, I.S., Mortimer, G.E., 1988. The petrology and geochemistry of granitic gneisses from the east Arunta Inlier, central Australia: implications for Proterozoic crustal development. Precambrian Res. 40/41, 233-259.

Foden J., Mawby J., Kelly S., Turner S., Bruce D., 1995. Metamorphic events in the eastern Arunta Inlier, Part 2. Nd-Sr-Ar isotopic constraints. Precambrian Res. 71, 207-227.

Foden, J., Song, S.H., Turner, S., Elburg, M., Smith, P.B., Van der Steldt, B., Penglis, D.V., 2001. Geochemical evolution of the lithospheric mantle beneath S.E. South Australia. Chem. Geol. In press.

Fodor, R.V., Vetter, S.K., 1984. Rift-zone magmatism; petrology of basaltic rocks transitional from CFB to MORB, southeastern Brazil margin. Contrib. Mineral. Petrol., 88, 307-321.

Fountain, D.M., Salisbury, M.H., 1981. Exposed cross-sections through the continental crust: implications for crustal structure, petrology, and evolution. Earth Plaet. Sci. Lett. 56, 263-277.

Furman, T., 1995. Melting of metasomatised subcontinental lithosphere: undersaturated mafic lavas from Rungwe, Tanzania. Contrib. Mineral. Petrol., 122, 97-115.

Garland, F., Turner, S., Hawkesworth, C., 1996. Shirts in the source of the Parana basalts through time. Lithos, 37, 223-243.

Gibson, S.A., Thompson, R.N., Dickin, A.P., Leonardos, O.H., 1996. Erratum to “high-Ti and low-Ti mafic potassic magmas: key to plume-lithosphere interactions and continental flood-basalt genesis”. Earth and Planet. Sci. Lett. 141, 325-341.

Glazner, A.F., Farmer, G.L., Hughes, W.T., Wooden, J.L., Pickthorn, W., 1991. Contamination of basaltic magma by the mafic crust at Amboy and Pisgah craters, Mojave Desert, California. J. Geophysical Res. 96, 13673-13691.

Green, D.H., Hibberson, W.O., Jaques, A.L., 1979. Petrogenesis of mid-ocean ridge basalts. In: McElhinny, M.W., (Ed.), The Earth: Its Origin, Structure and Evolution. Academic Press, London, pp 265-299.

Hajash, A., Jr, 1984. Rare earth element abundances and distribution patterns in hydrothermally altered basalts; experimental results. Contrib. Mineral. Petrol. 85, 409-412.

Hamilton, P.J., Evenson, N.M., O’Nions, R.K., Tarney, J., 1979. Sm-Nd systematics of Lewisian gneisses: implications for the origins of granulites. Nature, 277, 25-28.

Hand, M., Mawby, J., Kinny, P., Foden, J., 1999a. U-Pb ages from the Harts Range, central Australia; evidence for early Ordovician extension and constraints on Carboniferous metamorphism. J. Geol. Soc. (London) 156, 715-730.

Hand, M., Mawby, J., Miller, J.A., Ballevre, M., Hensen, B., Moller, A., Buick, I.S., 1999b. Tectonothermal evolution of the Harts and Strangways Range Region, eastern Arunta Inlier, central Australia. Specialist Group in Geochemistry, Mineralogy and Petrology Field Guide No. 4, Geol. Soc. Aust. p. 73.

Hanley, L.M., Wingate, M.T.D., 2000. SHRIMP zircon age for an early Cambrian dolerite dyke: an intrusive phase of the Antrim Plateau Volcanics of northern Australia. Aust. J. Earth. Sci. 47, 1029-1040.

Hansen, H., Nielsen, T.F.D., 1999. Crustal contamination in Palaeogene East Greenland flood basalts: plumbing system evolution during continental rifting. Chem. Geol. 157, 89-118.

Hawkesworth, C.J., Marsh, J.S., Duncan, A.R., Erlank, A.J., Norry, M.J., 1984. The role of continental lithosphere in the generation of the Karoo volcanic rocks; evidence from combined Nd and Sr isotopic studies. Geol. Soc. Sth. Africa Special Publication, 13, 341-354.

Hawkesworth, C.J., Galklagher, K., Kelley, S., Mantovani, M., Peate, D.W., Regelous, M., Rogers, N.W., 1992. Parana magmatism and the opening of the South Atlantic. In: Storey, B.C., Alabaster, T., Pankhurst, R.J. (Eds.), Magmatism and the causes of continental break-up. Geological Society Special Publication No. 68, pp. 221-240.

Hergt, J.M., Peate, D.W., Hawkesworth, C.J., 1991. The petrogenesis of Mesozoic Gondwana low-Ti flood basalts. Earth Planet. Sci. Lett. 105, 134-148.

Hooper, P.R., Hawkeswoth, C.J., 1993. Isotopic and geochemical constarints on the evolution of the Columbia River Basalt. J. Petrol. 34 1203-1246.

James, P.R., Ding, P., 1988. “Caterpillar tectonics” in the Harts Range area, a kinship between two sequential Proterozoic extensional collision orogenic belts within the eastern Arunta Inlier of central Australia. Precambrian Res. 40-41, 199-216.

Larsen, L.M., Watt, W.S., Watt, M., 1989. Geology and petrology of the lower Plateau Basalts of the Scoresby Sund region, East Greenland. Gronlands Geologiske Undersogelse Bull., 157, 1-164.

McDonough, W.F., 1990. Constraints on the composition of the continental lithospheric mantle. Earth Planet. Sci. Lett. 101, 1-18.

Mawby, J., Hand, M., Foden, J., 1999. Sm-Nd evidence for Ordovician granulite facies metamorphism in an intraplate setting in the Arunta Inlier, central Australia. J. Metamorphic Geol. 17, 653-668.

Mawby, J., 2000. Metamorphic and geochronologic consraints on Palaeozoic tectonism in the eastern Arunta Inlier. Unpublished PhD Thesis, Adelaide University.

Menzies, M.A., Hawkesworth, C.J., 1987. Upper mantle processes and compositions. In: Nixon, P.H., (Ed.), Mantle Xenoliths. Wiley, pp. 726-738.

Meschede, M., 1986. A method of discriminating between different types of mid-ocean ridge basalts and continental tholeiites with the Nb-Zr-Y diagram. Chem. Geol. 56, 207-218.

Miller, J.A., Cartwright, I., Buick, I.S., 1997. Granulite facies metamorphism in the Mallee Bore area, northern Harts Range; implications for the thermal evolution of the eastern Arunta Inlier, central Australia. J. Metamorphic Geol. 15, 613-629.

Mullen, E.D., 1983. $MnO/TiO_2/P_2O_5$: a minor element discriminant for basaltic rocks of oceanic environments and its implications for petrogenesis. Earth Planet. Sci.Lett., 62, 53-62.

Oxburg, E.R., Parmentier, E.M., 1978. Thermal processes in the formation of continental lithosphere, Philos. Trans. R. Soc. London, 288, 415-429.

Paslick, C., Halliday, A., James, D., Dawson, J.B., 1995. Enrichment of the continental lithosphere by OIB melts: Isotopic evidence from the volcanic province of northern Tanzania. Earth Planet. Sci. Lett. 130, 109-126.

Pearce, J.A., 1983. Role of the sub-continental lithosphere in magma genesis at active continental margins. In; Hawkeswroth, C.J., Norry, M.J., (Eds.), Continental basalts and mantle xenoliths. Nantwich, England, Shiva, p 215-246.

Pearce, J.A., Cann, J.C., 1973. Tectonic setting of basic volcanic rocks determined using trace element analyses. Earth Planet. Sci. Lett. 19, 290-300.

Peng, Z.X., Mahoney, J., Hooper, P., Harris, C., Beane, J., 1994. A role for lower continental crust in flood basalt genesis? Isotopic and incompatible element study of the lower six formations of the western Deccan Traps. Cosmica et Cosmochimica Acta, 58, 267-288.

Pinese, J.P.P., Teixeira, W., Piccirillo, E.M., Quemeneur, J.J.G., Bellieni, G., 1995. In: Baer, G., Heimann, A. (Eds.), Physics and Chemistry of Dykes. Balkena, Rotterdam, pp. 205-218.

Powell, R., Holland, T., 1988. An internally consistent dataset with uncertainties and correlations: 3. Applications to geobarometry, worked examples and a computer program. J. Metamorphic Geol. 6, 173-204.

Rochell, A., Stein, M., Molzahn, M., Hart, S.R., Worner, G., 1995. Geochemical evolution of rift magmas by progressive tapping of a stratified mantle source beneath the Ross Sea Rift, northern Victria Land, Antarctica. Earth Planet. Sci. Lett. 131, 207-224.

Rogers, N., Macdonald, R., Fitton, J.G., George, R., Smith, M., Barreiro, B., 2000. Two mantle plumes beneath the East African rift system: Sr, Nd and Pb isotope evidence from Kenya Rift basalts. Earth Planet. Sci. Lett. 176, 387-400.

Rushmer, T., 1991. Partial melting of two amphibolites: contrasting experimental results under fluid-absent conditions. Contrib. Mineral. Petrol. 107, 41-59.

Saunders, A.D., Tarney, J., Weaver, S.D., 1980. Transverse geochemical variations across the Antarctic Peninsula: implications for the genesis of calc-alkaline magmas. Earth Planet. Sci. Lett. 46, 344-360.

Schmitz, M.D., Wirth, K.R., Craddock, J.P., 1995. Major and trace element geochemistry of early Proterozoic mafic dykes of northern Minnesota and south western Ontario. In: Baer, G., Heimann, A. (Eds.), Physics and Chemistry of Dykes. Balkena, Rotterdam, pp. 219-233.

Sheraton, J.W., Black, L.P., McCulloch, M.T., Oliver, R.L., 1990. Age and origin of a compositionally varied mafic dyke swarm in the Bunger Hills, East Antarctica. Chem. Geol. 85, 215-246.

Sivell, W.J., 1988. Geochemistry of metatholeiites from the Harts Range, Central Australia: implications for mantle source heterogenity in a Proterozoic mobile belt. Precambrian Res. 40/41, 261-275.

Sivell, W.J., Foden, J.D., 1985. Banded amphibolites of the Harts Range Meta-igneous Complex, Central Australia: an early Proterozoic basalt-tonalite suite. Precambrian Res. 28, 223-252.

Sivell, W.J., Foden, J.D., Lawrence, R.W., 1985. The Entire anorthositic gneiss, eastern Arunta Inlier, Central Australia: geochemistry and petrogenesis. Aust. J. Earth Sci. 32, 449-465.

Sivell, W.J., McCulloch, M.T., 1991. Neodymium isotope evidence for ultra-depleted mantle in the early Proterozoic. Nature, 354, 384-386.

Spath, A., Le Roex, A.P., Opiyo-Akech, N., 2001. Plume-lithosphere interaction and the origin of continental rift-related alkaline volcanism – the Chyulu Hills Volcanic Province, southern Kenya. J. Petrol. 42, 765-787.

Stakes, D.S., Shervais, J.W., Hopson, C.A., 1984. The volcanic-tectonic cycle of the Famous and Amar valleys, Mid-Atlantic Ridge (34°47'N): Evidence from basalt glass and phenocryst compositional variations for a steady state magma chamber beneath the valley midsection, Amar 3. J. Geophysical Res. 89, 6995-7028.

Stanley, C.R., Russell, J.K., 1989. Petrologic hypothesis testing with Pearce element ratio diagrams: derivation of diagram axes. Contrib. Mineral. Petrol. 103, 78-89.

Storey, B.C., Leat, P.T., Weaver, S.D., Pankhurst, R.J., Bradshaw, J.D., Kelley, S., 1999. Mantle plumes and Antarctica-New Zealand rifting: evidence from mid-Cretaceous mafic dykes. J. Geol. Soc. (London) 156, 659-671.

Sun, S.-S., McDonough, W.F., 1989. Chemical and isotopic systematics of oceanic basalts: implications for mantle composition and processes. In: Saunders, A.D., Norry, M.J. (Eds.), Magmatism in the Ocean Basins. Geol. Soc. Spec. Publ., vol. 42, pp 313-345.

Thompson, R.N., Gibson, S.A., Leat, P.T., Mitchell, J.G., Morrison, M.A., Hendry, G.L., Dickin, A.P., 1993. Early Miocene continental extension-related basaltic magmatism at Walton Peak, northwest Colorado: further evidence on continental basalt genesis. J. Geol. Soc. (London) 150, 277-292.

Thompson, R.N., Gibson, S.A., 1994. Magmatic expression of lithospheric thinning across continental rifts. Tectonophysics, 233, 41-68.

Townson, W.G., 1985. The subsurface geology of the western Officer Basin; results of Shell's 1980-1984 petroleum exploration campaign. APEA Journal, 25, 34-51.

Treuil, M., Varet, J., 1973. Criteres volcanogiques, petrologiques et geochemiques de la genese et de la differentiation des magmas basaltiques: exemple de l'Afar. Bull. Geol. Soc. France, 7th Ser., 15, 401-644

Turner, S., 1996. Petrogenesis of the late-Delamerian gabbroic complex at Black Hill, South australia : implications for convective thinning of the lithospheric mantle. Mineral. Petrol. 56, 51-89.

Turner, S., Foden, J.D., 1990. Magma mingling in late-Delamerian A-type granites at Mannum, South Australia. Mineral. Petrol. 56, 147-169.

Turner, S., Hawkesworth, C., Gallagher, K., Stewart, K., Peate, D., Mantovani, M., 1996. Mantle plumes, flood basalts, and thermal models for melt generation beneath continents : assessment of a conductive heating model and application to the Parana. J. Geophysical Res. 101, 11503-11518.

Wareham, C.D., Stump, E., Story, B.C., Millar, I.L., Riley, T.R., 2001. Petrogenesis of the Cambrian Liv Group, a bimodal volcanic rock suite from the Ross Orogen, Transantarctic Mountains. Geol. Soc. America Bull. 113, 360-372.

Weaver, B.L. Tarney, J., 1981. Chemical changes during dyke metamorphism in high grade basement terrains. Nature, 289, 47-49.

White, W.M., Hofmann, A.W., 1982. Sr and Nd isotope geochemistry of oceanic basalts and mantle evolution. Nature, 296, 821-825.

Windrum, D.P., McCulloch, M.T., 1986. Nd and Sr isotopic systematics of central Australian granulites : chronology of crustal development and constraints on the evolution of lower continental crust. Contrib. Mineral. Petrol. 94, 289-303.

Wirth, K.R., Vervoort, J.D., 1995. Nd isotopic constraints on mantle and crustal contributions to Early Proterozoic dykes of the southern Superior Province. In: Baer, G., Heimann, A. (Eds.), Physics and Chemistry of Dykes. Balkena, Rotterdam. pp. 237-249.

Wittke, J.H., Smith, D., Wooden, J.L., 1989. Origin of Sr, Nd and Pb isotopic systematics in high-Sr basalts from central Arizona. Contib. Mineral. Petrol. 101, 57-68.

Wolf, M.B., Wyllie, P.J., 1994. Dehydration-melting of amphibolite at 10kbar: the affects of temperature and time. Contrib. Mineral. Petrol. 115, 369-383.

Zhao, J.-X., 1992. Proterozoic crust-mantle evolution in central Australia: geochemical and isotopic constraints. Unpublished PhD Thesis, Adelaide University.

Zhao, J.-X., McCulloch, M.T., 1993a. Melting of a subduction-modified continental lithospheric mantle: Evidence from Late Proterozoic mafic dike swarms in central Australia. Geology, 21, 463-466.

Zhao, J.-X., McCulloch, M.T., 1993b. Sm-Nd isochron ages of late Proterozoic dyke swarms in Australia: evidence for two distinctive events of mafic magmatism and crustal extension. Chem. Geol. 109, 341-354.

Zhao, J.-X., McCulloch, M.T., Korsch, R.J., 1994. Characterisation of a plume-related ~800 Ma magmatic event and its implication for basin for basin formation in central-southern Australia. Earth Planet. Sci. Lett. 121, 349-367.

Zwaan, K.B., Van Roermund, H.L.M., 1990. A firt-related mafic dyke swarm in the Corrovarre Nappe of the Caledonian Middle Allochthon, Troms, North Norway, and its tectonometamorphic evolution. Nor. Geol. Unders. Bull., 419, 25-44.

Table 1

Major and trace element data for the Group 1 Harts Range Dykes.

Sample:	GH2	GH4	GH5	LAD1	LAD6	LAD12A	LAD14	LAD19	LAD2A	LAD42	LAD6A	MD1A	MD8	NHRD	NHRD10A	NHRD10B	NHRD5	NHRD6	NHRD7A	NHRD9
SiO_2	48.40	48.43	49.06	48.74	50.96	48.75	48.99	48.34	49.12	49.40	48.88	48.33	49.08	48.04	48.76	49.08	49.22	48.22	50.64	48.39
Al_2O_3	15.48	16.06	15.41	14.27	13.94	15.42	15.70	16.61	16.19	14.41	14.30	16.91	14.37	13.41	14.47	15.84	14.10	15.70	14.15	17.45
Fe_2O_3T	10.76	10.21	11.73	12.40	15.42	11.79	10.43	10.60	11.02	12.42	12.36	10.21	12.67	15.27	13.04	12.14	12.65	9.64	14.17	9.72
MnO	0.17	0.16	0.18	0.20	0.21	0.18	0.17	0.17	0.18	0.19	0.20	0.16	0.20	0.24	0.20	0.18	0.20	0.15	0.22	0.15
MgO	8.96	8.91	7.28	7.66	7.71	7.77	8.31	7.13	6.75	7.53	7.70	6.79	7.59	6.62	7.43	6.33	7.13	9.65	6.70	8.11
CaO	12.29	12.51	12.29	11.90	9.75	12.14	12.48	12.20	12.16	11.95	12.03	12.09	11.88	9.75	11.21	11.73	11.09	12.54	10.99	12.66
Na_2O	2.42	2.24	2.47	2.57	0.70	2.64	2.41	2.37	2.86	2.33	2.47	2.83	1.54	2.21	2.52	2.58	2.65	1.91	0.75	2.11
K_2O	0.11	0.10	0.16	0.19	0.07	0.13	0.12	0.19	0.21	0.16	0.14	0.19	0.19	0.56	0.18	0.26	0.22	0.12	0.24	0.14
TiO_2	1.37	1.21	1.63	1.77	1.74	1.59	1.24	1.52	1.73	1.60	1.75	1.51	1.85	2.59	2.03	1.90	1.95	0.91	2.32	1.18
P_2O_5	0.14	0.12	0.15	0.17	0.11	0.15	0.12	0.16	0.18	0.16	0.17	0.15	0.18	0.27	0.20	0.21	0.20	0.09	0.23	0.12
SO_3	0.03	0.02	0.10	0.14	0.05	0.04	0.02	0.09	0.04	0.05	0.20	0.14	0.09	0.01	0.11	0.04	0.02	0.02	0.03	0.05
LOI	0.00	0.10	-0.03	0.19	-0.40	-0.01	0.15	0.39	0.01	-0.20	0.16	0.53	0.42	0.43	0.09	0.03	0.33	0.51	-0.05	0.17
Total	100.13	100.07	100.43	100.20	100.26	100.59	100.14	99.77	100.45	100.00	100.36	99.84	100.06	99.40	100.24	100.32	99.76	99.46	100.39	100.25
Mg#	62.25	63.35	55.14	55.02	49.75	56.62	61.21	57.12	54.81	54.56	55.23	56.84	54.26	46.20	53.02	50.80	52.75	66.47	48.36	62.30
Zr	94	79	102	111	78	101	79	105	125	106	113	111	122	184	140	146	132	48	164	79
Nb	2.1	1.5	1.1	2.8	2.3	2.0	1.4	3.3	3.2	1.7	1.9	2.9	3.0	3.5	3.2	3.5	2.1	0.5	4.2	0.3
Y	34	30	35	41	27	37	30	34	37	38	40	34	43	62	47	44	45	22	50	28
Sr	129	127	146	130	149	135	134	166	199	135	123	179	129	140	136	143	149	86	157	145
Rb	1.8	2.8	2.7	9.2	2.4	2.5	2.2	4.3	3.7	4.3	2.8	5.8	3.7	7.1	3.8	7.0	3.7	2.5	4.0	4.0
U	0.2	0.0	0.7	0.0	0.1	0.2	0.6	0.3	2.0	1.2	0.8	0.3	0.7	0.0	0.0	1.9	0.6	0.0	0.5	1.4
Th	1.7	1.6	3.6	2.1	1.7	2.1	2.7	1.6	2.9	1.4	1.6	1.4	0.6	2.3	2.6	2.0	3.6	0.6	2.4	0.8
Pb	1.4	0.3	2.2	26.3	3.8	1.5	1.7	4.2	2.1	0.0	1.2	3.1	4.0	6.8	3.9	1.5	0.0	3.0	2.6	4.6
Ga	17	16	18	21	24	18	16	18	18	20	17	18	18	20	20	20	20	14	21	17
Cu	72	66	55	65	77	71	74	48	69	53	69	66	64	62	63	67	62	64	65	81
Zn	71	68	80	105	133	78	70	79	73	87	84	71	94	119	96	90	93	66	107	74
Ni	135	128	60	85	164	96	115	79	49	53	80	71	84	79	86	53	68	183	63	115
Ba	14	13	14	45	131	14	103	74	30	16	15	24	76	115	15	23	150	14	133	111
Sc	37	37	38	42	33	39	37	37	39	42	43	35	44	44	36	35	45	37	41	33
Co	61	62	54	64	74	55	64	55	52	74	56	54	63	67	62	59	64	68	81	63
V	280	264	344	364	283	323	282	296	311	346	367	283	377	458	372	346	386	249	431	249
Ce	13	8	20	20	28	9	13	18	19	19	20	21	19	28	21	25	24	9	26	12
Nd	10	12	11	12	11	14	10	12	12	12	14	14	12	23	17	15	16	9	19	9
La	1	2	2	6	7	2	3	2	5	2	4	5	4	8	8	5	5	3	6	1
Cr	443	495	214	340	375	295	396	290	211	208	328	272	294	213	301	205	186	526	88	388
Zr/Nb	44.8	52.8	92.6	39.8	34.1	50.4	56.3	31.8	39.2	62.3	59.4	38.2	40.6	52.6	43.6	41.7	63.1	96.1	39.2	263.8
Th/Nb	0.82	1.08	3.31	0.76	0.75	1.06	1.95	0.49	0.92	0.83	0.85	0.49	0.20	0.67	0.82	0.58	1.73	1.21	0.58	2.70
Zr/Y	2.78	2.68	2.90	2.75	2.87	2.71	2.65	3.12	3.40	2.79	2.79	3.27	2.84	2.96	2.94	3.33	2.98	2.14	3.26	2.78

All oxide values are expressed as wt %. Trace elements expressed as ppm. Co is subject to mill contamination. All zero values represent values which fall below detection limits.

Mg# = [100 x Mg^{2+} / (Mg^{2+} + ΣFe)]. LOI: denotes loss on ignition.

Table 2

Major and trace element data for the Group 2 Harts Range Dykes.

Sample:	LAD11	LAD39	LAD43	LAD4A	LAD5	NHRD7	LAD21-1	LAD10A	GS1	GS4	GS5	GS6	GS7	LAD14A	LAD21	LAD27	LAD28	LAD29	LAD3	LAD32	LAD36
SiO_2	44.35	49.51	51.19	52.34	49.97	50.91	45.74	51.71	49.40	45.53	49.21	49.57	50.39	46.54	46.16	50.42	49.96	51.72	49.67	48.60	52.21
Al_2O_3	14.63	13.91	12.65	13.21	13.13	17.07	11.63	15.64	17.11	13.45	16.61	16.60	17.62	17.53	12.32	12.64	12.99	15.34	14.72	10.83	13.13
Fe_2O_3T	17.62	13.50	15.00	14.50	15.73	11.06	13.27	13.79	11.93	21.19	11.78	11.82	10.19	15.26	13.83	13.58	13.55	13.22	11.33	12.00	13.65
MnO	0.24	0.21	0.22	0.21	0.22	0.18	0.20	0.20	0.18	0.27	0.18	0.18	0.17	0.25	0.24	0.21	0.21	0.19	0.19	0.21	0.24
MgO	8.55	7.64	9.03	8.98	8.74	7.09	10.45	6.74	7.34	5.61	7.81	7.91	7.35	7.44	10.25	11.85	11.05	7.44	9.63	14.14	7.74
CaO	11.33	12.54	8.66	8.77	9.46	10.12	14.03	10.30	9.43	9.02	10.12	10.36	10.36	11.37	12.76	7.73	8.04	10.00	11.49	10.69	10.41
Na_2O	0.72	1.62	1.80	0.73	1.14	2.06	1.23	1.16	2.18	0.91	2.11	2.20	2.35	0.86	1.33	1.52	1.63	0.96	1.32	0.57	0.95
K_2O	0.19	0.20	0.30	0.11	0.24	0.54	0.62	0.15	0.85	0.65	0.58	0.56	0.64	0.09	0.71	0.61	0.91	0.12	0.34	1.16	0.10
TiO_2	2.88	0.90	1.52	1.47	1.63	0.95	1.66	1.25	1.23	2.16	0.85	0.83	0.67	1.47	1.11	0.87	0.98	1.21	0.82	0.70	1.44
P_2O_5	0.27	0.09	0.09	0.09	0.10	0.13	0.13	0.10	0.26	0.30	0.16	0.15	0.16	0.32	0.24	0.16	0.17	0.16	0.12	0.15	0.25
SO_3	0.01	0.02	0.02	0.10	0.08	0.01	0.05	0.07	0.03	0.38	0.14	0.12	0.14	0.07	0.14	0.01	0.02	0.04	0.10	0.11	0.16
LOI	-0.46	0.01	-0.37	-0.20	-0.31	-0.10	0.50	-0.39	0.19	0.19	0.63	0.16	0.34	-0.36	0.49	-0.08	0.06	-0.27	0.29	0.28	-0.10
Total	100.33	100.15	100.11	100.31	100.13	100.02	99.51	100.72	100.13	99.66	100.18	100.46	100.38	100.84	99.58	99.52	99.57	100.13	100.02	99.44	100.18
Mg#	49.01	52.85	54.38	55.09	52.39	55.94	60.93	49.19	54.92	34.40	56.77	57.00	58.82	49.12	59.48	63.34	61.76	52.71	62.73	70.00	52.90
Zr	140	67	67	65	67	62	79	56	115	147	80	72	77	49	104	65	90	103	86	66	88
Nb	13.7	3.7	3.1	3.4	2.7	4.3	7.4	4.5	9.4	10.6	4.9	4.7	6.5	7.9	16.1	5.0	7.1	6.7	8.0	5.3	15.6
Y	31	28	23	24	26	25	19	24	26	41	19	19	16	32	29	19	22	23	25	22	39
Sr	518	115	129	134	150	188	223	155	301	198	248	250	294	455	575	145	148	202	290	247	459
Rb	3.8	3.8	6.0	2.7	10.0	11.6	7.7	1.1	30.2	22.7	17.1	17.6	16.7	1.0	6.7	24.0	40.3	3.0	13.5	57.0	1.9
U	0.8	1.0	0.9	1.4	0.9	0.0	0.9	0.7	0.9	2.3	0.0	0.5	0.4	1.1	3.0	1.4	0.5	0.2	1.4	0.0	0.0
Th	0.5	1.7	1.7	3.1	1.9	1.5	2.9	1.8	4.7	3.8	2.9	3.1	3.2	1.8	2.5	0.7	3.1	1.9	2.5	2.7	0.7
Pb	5.0	8.9	8.5	10.9	2.7	11.3	4.6	2.4	5.8	19.2	7.1	4.2	3.5	4.5	5.1	3.3	3.8	2.6	5.8	3.0	6.6
Ga	25	18	22	20	24	18	18	23	19	24	17	17	19	26	16	16	17	18	17	13	18
Cu	38	138	83	77	74	70	23	35	52	207	64	66	57	46	88	88	61	21	47	68	28
Zn	125	93	133	144	131	991	94	105	91	179	83	76	69	110	104	108	120	102	82	87	99
Ni	189	69	227	230	182	171	242	124	148	123	153	140	120	16	139	382	378	158	184	158	71
Ba	179	56	76	81	115	213	444	72	360	357	236	249	268	68	187	325	257	159	294	344	113
Sc	44	51	33	33	34	27	56	30	30	40	32	30	27	41	45	30	30	30	41	38	40
Co	84	77	70	68	65	67	71	59	62	86	64	61	56	57	63	68	67	62	61	64	55
V	503	311	269	265	282	188	391	256	208	491	194	196	145	353	322	208	210	227	250	269	333
Ce	32	19	18	22	13	20	18	22	62	79	40	34	37	46	85	29	40	37	39	29	66
Nd	27	11	7	9	7	14	13	7	27	34	16	14	18	26	48	18	22	16	21	21	48
La	10	5	3	6	4	8	5	5	29	33	15	14	16	18	30	14	15	13	12	15	24
Cr	422	34	599	627	558	320	1426	194	200	8	184	143	85	29	851	880	829	303	867	2121	447
Zr/Nb	10.2	18.1	21.5	19.2	25.0	14.5	10.6	12.5	12.3	13.8	16.2	15.4	11.8	6.2	6.4	13.0	12.7	15.3	10.7	12.4	5.7
Th/Nb	0.04	0.46	0.55	0.92	0.71	0.35	0.40	0.40	0.50	0.36	0.60	0.67	0.50	0.23	0.16	0.14	0.44	0.29	0.32	0.52	0.05
Zr/Y	4.47	2.36	2.87	2.69	2.59	2.50	4.11	2.34	4.53	3.56	4.30	3.84	4.72	1.56	3.64	3.41	4.00	4.37	3.37	3.00	2.29

All oxide values are expressed as wt %. Trace elements expressed as ppm. Co is subject to mill contamination. All zero values represent values which fall below detection limits.

Mg# = [100 x Mg^{2+} / (Mg^{2+} + ΣFe)]. LOI: denotes loss on ignition.

Table 3

Rare-earth element data for representative samples of the Group 1 and 2 Harts Range Dykes.

Sample:	NHRD10A	MD1A	MD8	LAD1	LAD6	LAD14	LAD42	LAD6A	LAD11	LAD28	LAD4A	GS6	GS7	NHRD7
Group:	1	1	1	1	1	1	1	1	2	2	2	2	2	2
Ce	15	12	12	12	14	8	11	12	25	28	11	25	28	19
La	6	5	4	4	7	3	4	4	10	15	5	13	16	10
Dy	6.5	4.5	5.5	5.5	3.5	4	5.5	5.5	4.5	3.5	4	2.5	2.5	3.5
Er	4	3	4	3	2	3	3	3	2	2	2	2	2	2
Eu	1.5	1	1.5	1.5	1	1	1.5	1	2	1	1	1	1	1
Gd	5	4	4	4	3	3	4	4	5	3	3	3	3	3
Ho	1.5	1	1.5	1.5	1	1	1	1	1	0.5	1	0.5	0.5	0.5
Nd	14.5	10.5	11.5	11.5	9.5	8	10	11	20	18	8.5	14.5	15	12.5
Pr	2	2	2	2	2	1	2	2	4	4	2	4	4	3
Sm	5	3	4.5	4	3.5	3	3.5	4	5.5	4.5	2.5	3	3	3.5
Yb	4	3	3	3	2	2	3	3	2	2	2	1	1	2

All rare-earth elements expressed as ppm.

Table 4
Sm-Nd and Rb-Sr isotope data for the HRD.

Sample	Group	Sm (ppm)	Nd (ppm)	$^{147}Sm/^{144}Nd$	$^{143}Nd/^{144}Nd$	$\varepsilon_{Nd}(480)$	Rb (ppm)	Sr (ppm)	$^{87}Rb/^{86}Sr$	$^{87}Sr/^{86}Sr$
NHRD 6	1	1.96	5.47	0.21662	0.512260	5.3	2.0	86	0.067	0.703568
NHRD10B	1	4.54	14.15	0.19388	0.512328	6.7	6.3	141	0.130	0.703281
LAD 4A	2	2.55	7.89	0.19552	0.511881	-2.1	1.9	132	0.014	0.710377
LAD 11	2	5.69	21.53	0.15975	0.511986	0.0	3.0	506	0.017	0.704807
LAD 28	2	4.04	17.73	0.13782	0.511400	-11.5	38.7	146	0.766	0.717247

Table 5

Comparison of various continental lithospheric sources.

Sample:	Group 2 - HRD	Stuart Dyke Swarm	Colorado Plateau	Avg CLM	Parana CFBs
Reference:	This study	Zhao & McCulloch, 1993	Wittke et al., 1989	McDonough, 1990	Hawkesworth et al., 1992
Zr	83	56	209	21	166
Sr	260	150	2194	49	238
Rb	14	33	28	2	45
Ba	212	163	1437	33	388
Zr/Ba	0.52	0.41	0.15	0.64	0.43
La/Nb	1.98	2.18	2.96	0.54	-
K_2O	0.46	0.54	2.58	0.054	1.33
K_2O/TiO_2	0.46	0.84	1.84	0.6	0.93

Stuart Dyke Swarm - subduction modified continental lithospheric mantle

Colorado Plateau - subduction modified continental lithospheric mantle

Avg CLM - average continental lithospheric mantle

Parana CFBs - unmodified continental lithospheric mantle

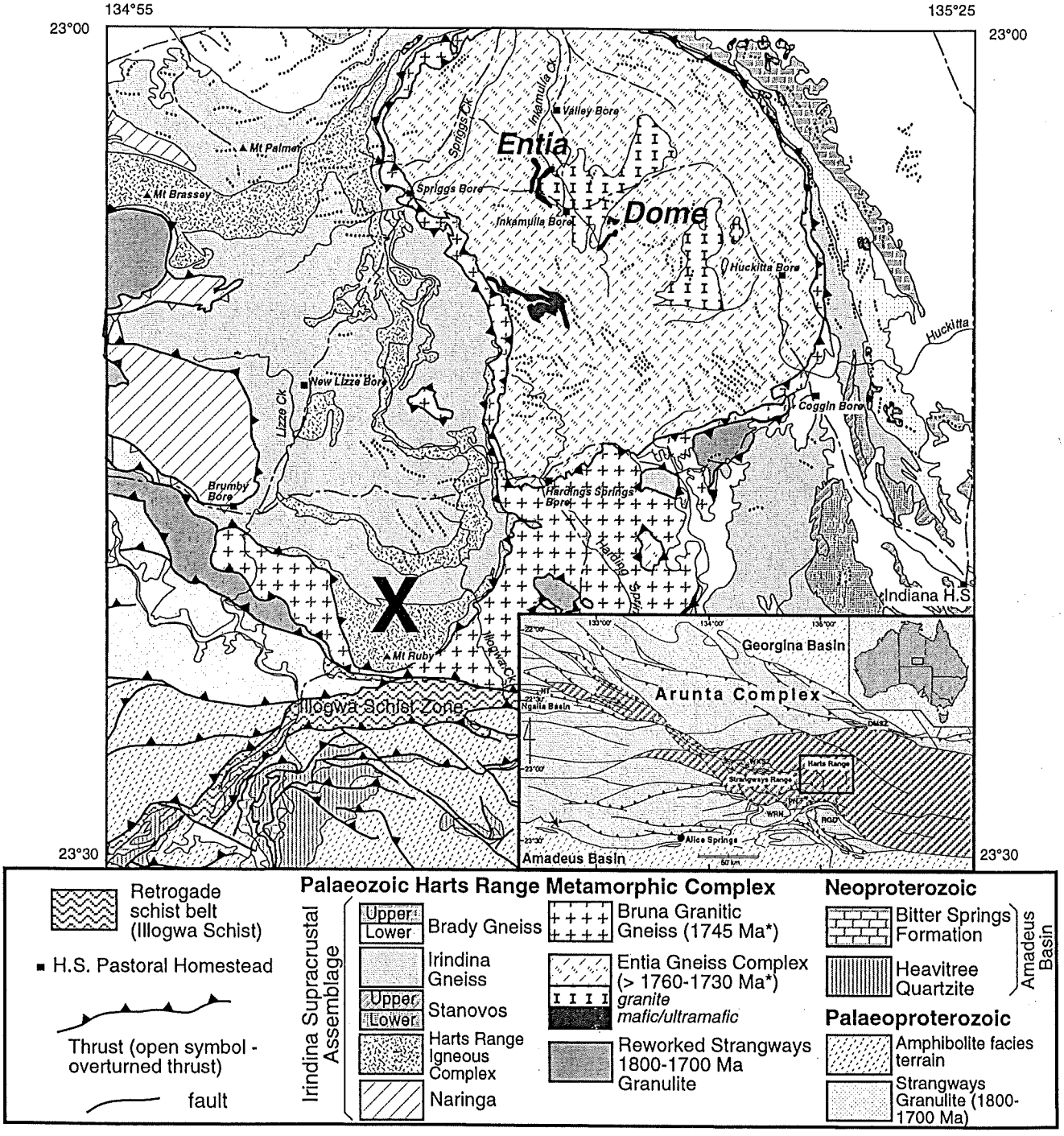

Fig. 1. Geological map of the Harts Range, eastern Arunta Block, showing structural relationships between the Palaeoproterozoic Strangways Metamorphic Complex and the Entia Gneiss Complex, with the early Cambrian Irindina Supracrustal Assemblage (Buick et al., 2001b). 'X' marks the position of Fig. 3.

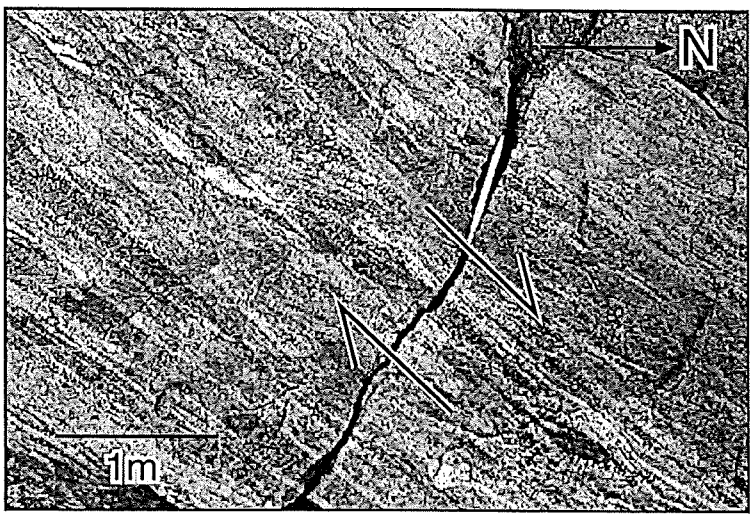

Fig. 2. Photo of the D2 extensional shear bands, indicating top to the north shear sense.

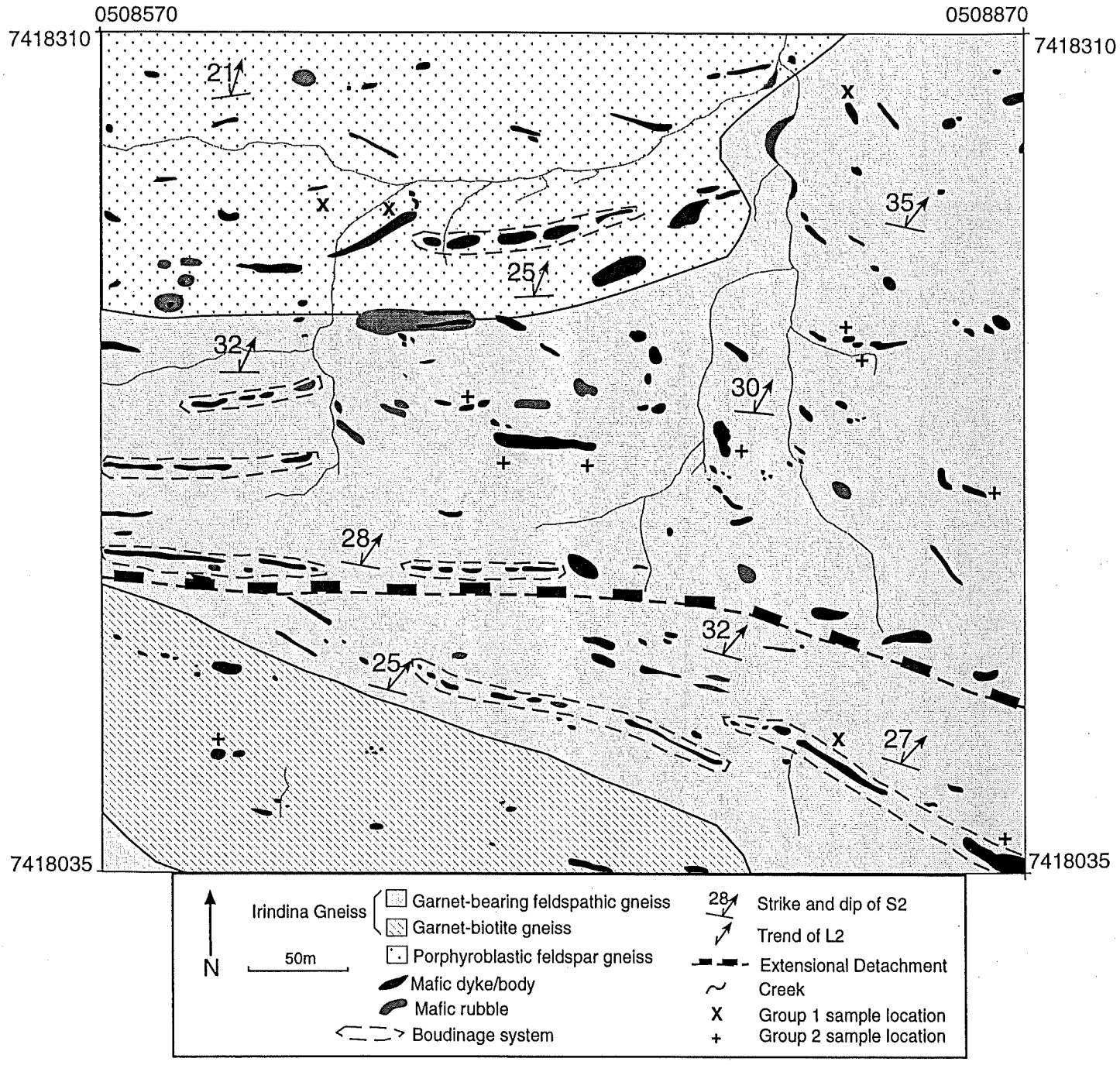

Fig. 3. Simplified geological map of a region north of Mt. Ruby, illustrating the near parallel relationship between the S2 fabric formed during near isothermal decompression of the terrane during early Ordovician N-S extension (Mawby et al., 1999), and sills and dykes belonging to the HRD. The total list of sample locations of analysed dykes are contained in Appendix D.

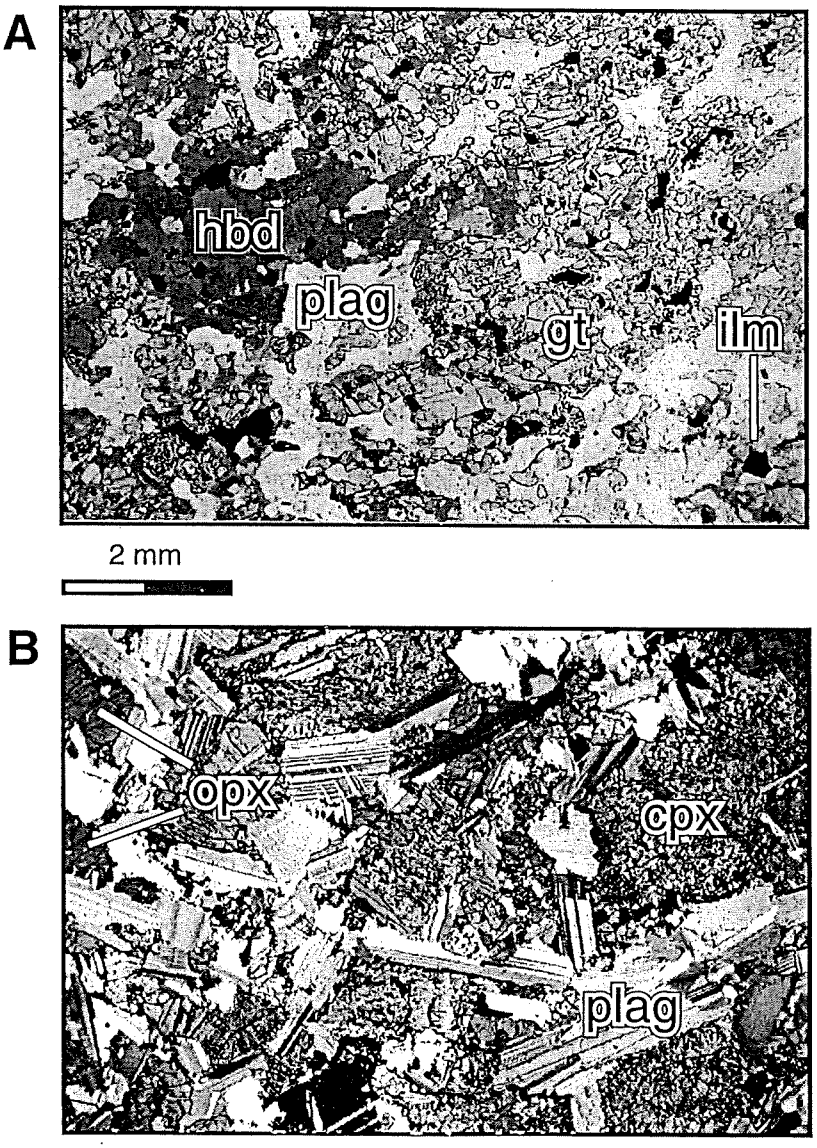

Fig. 4. **A:** Photomicrograph of an extensively recrystallised Harts Range Dyke. **B:** Photomicrograph of a dyke which preserves most of its original igneous nature as indicated by the relic plagioclase grains.

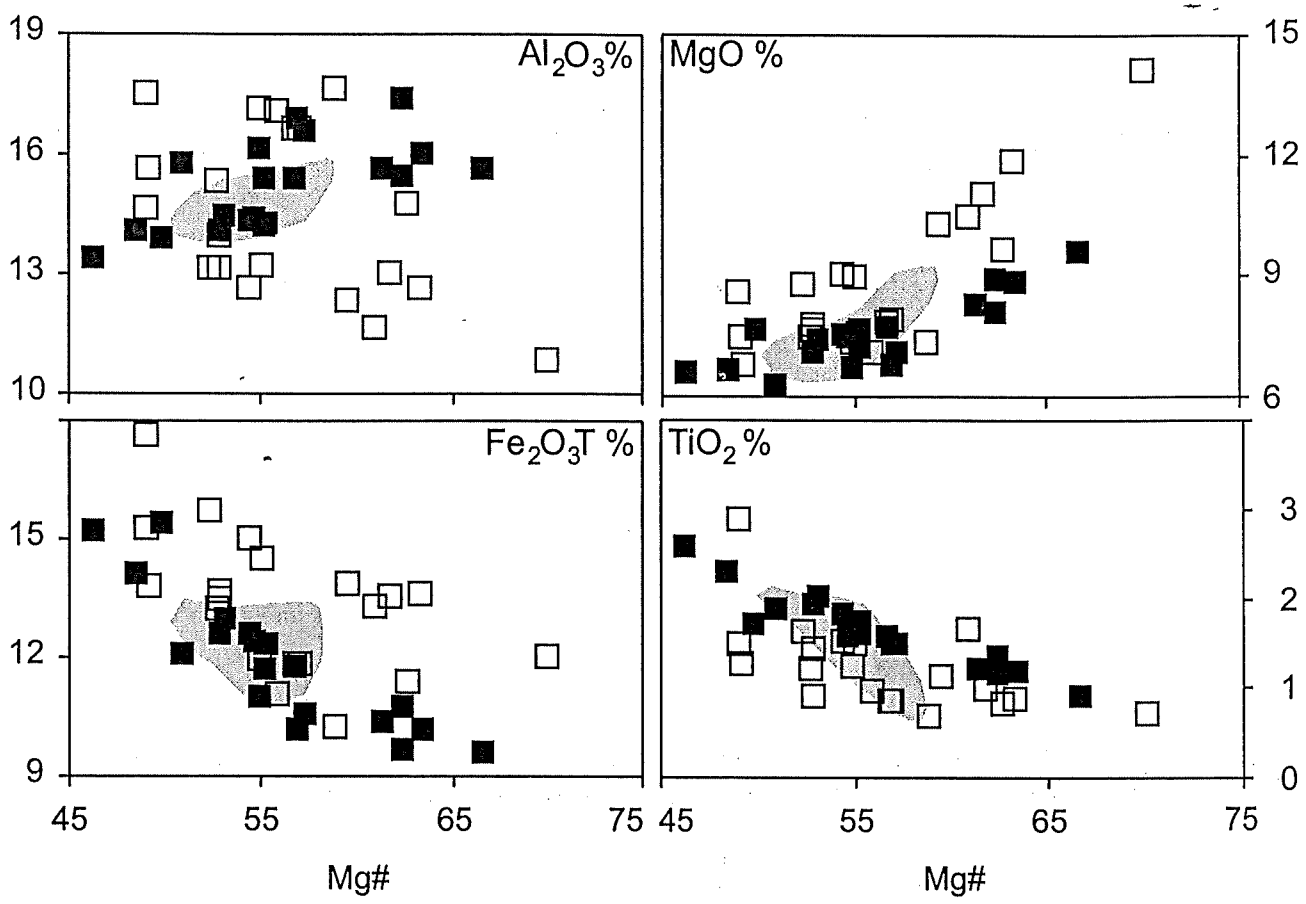

Fig. 5. Major element oxide diagrams plotted against Mg#, indicating the trends associated with fractional crystallisation of olivine, pyroxene and plagioclase. Solid squares are the Group 1 dykes and unfilled squares are the Group 2 dykes. Shaded areas represent values for the Harts Range Meta-tholeiites (Sivell, 1988).

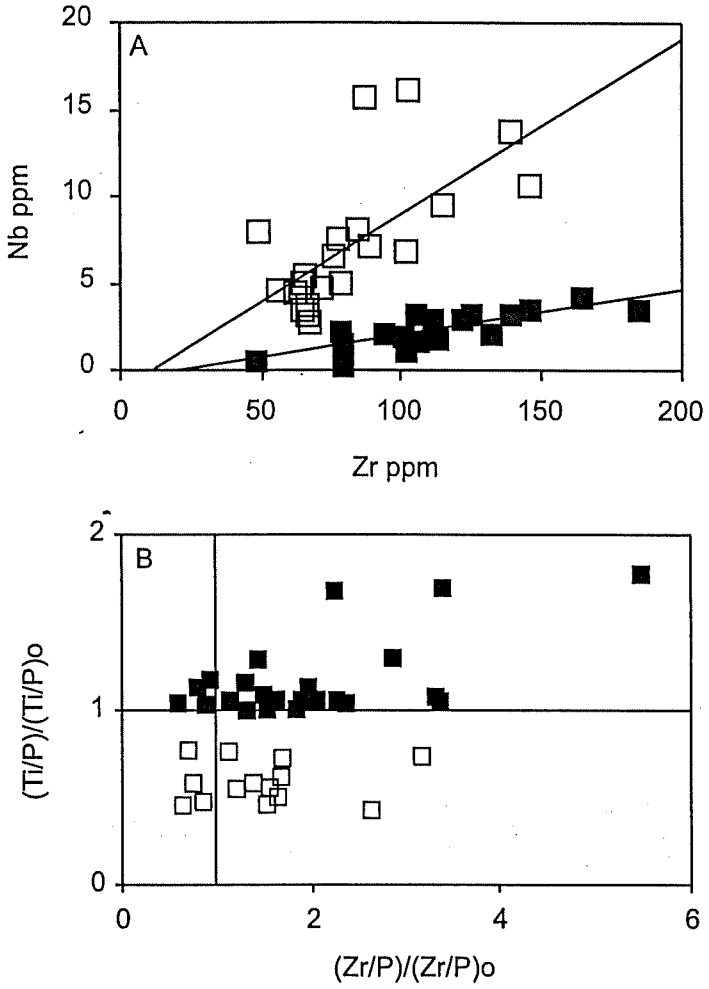

Fig. 6. **A**: Zr plotted against Nb indicating the fractionation trends of two separate, cogenetic groups. **B**: Pearce Element Ratio plot which also categories two separate cogenetic groups of HRD. Solid squares are the Group 1 dykes and unfilled squares are the Group 2 dykes.

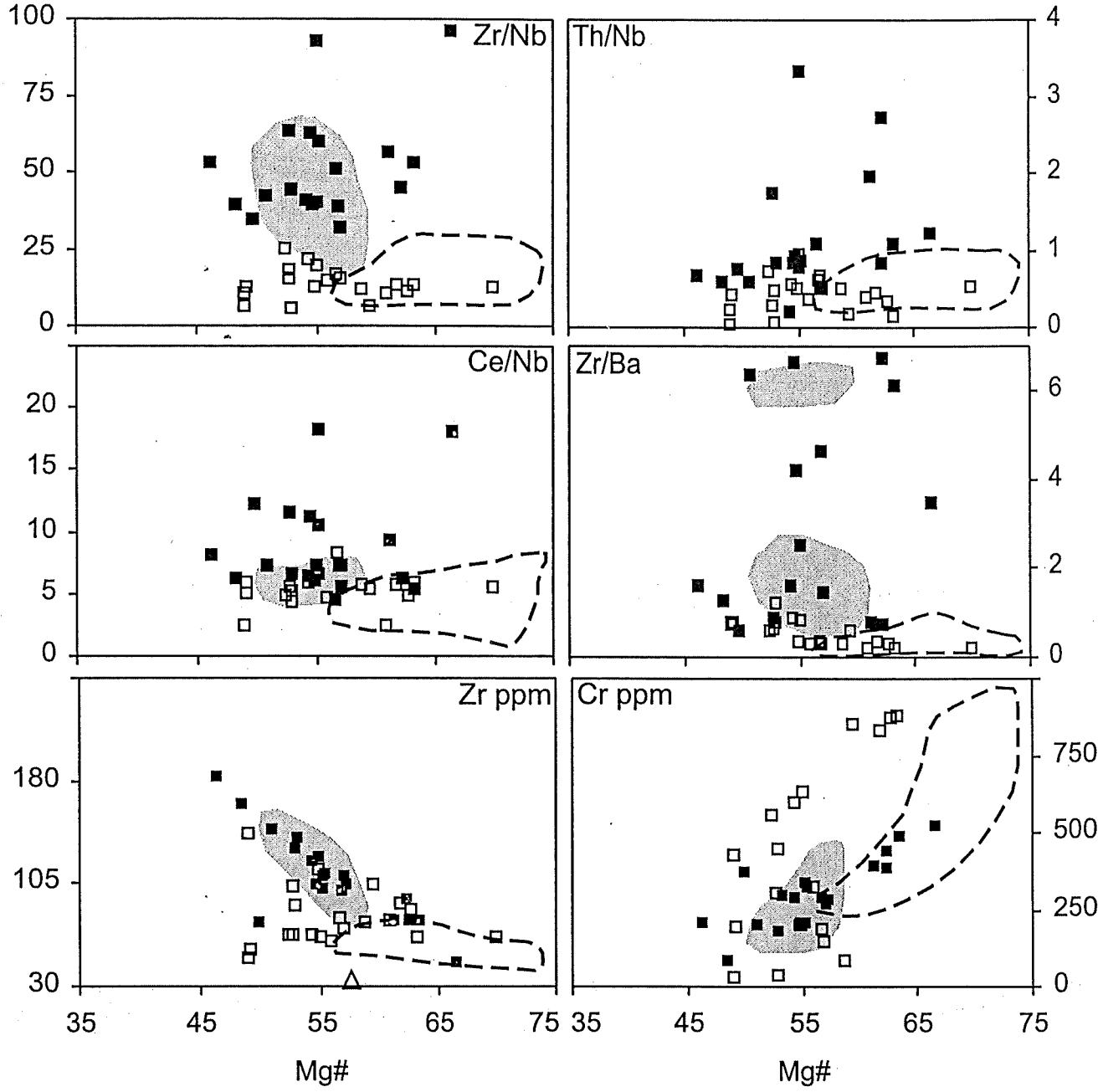

Fig. 7. Trace element abundances plotted against Mg#, illustrating the differences between the Group 1 dykes and the Group 2 dykes. Symbols as in Fig. 5. Dashed fields are data from Zhao (1993). Shaded area represent values for the Harts Range Meta-tholeiites (Sivell, 1988).

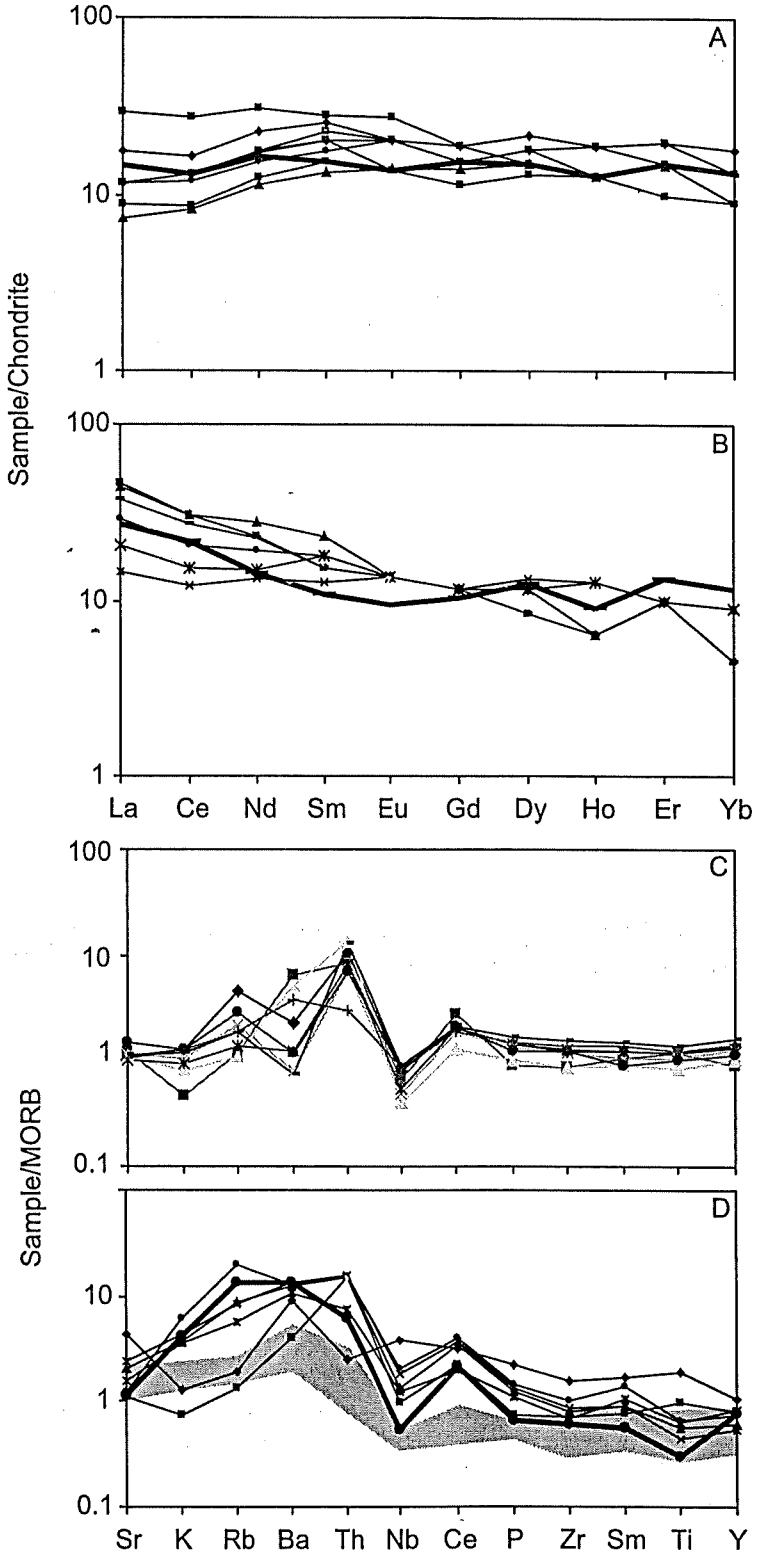

Fig. 8. **A**: Chondrite normalised REE pattern of the Group 1 dykes showing the pattern of N-type MORB (Sun and McDonough, 1989). **B**: REE pattern of the Group 2 dykes highlighting a subduction-modified CLM (Zhao and McCulloch, 1993). **C**: Incompatible trace element diagram of the Group 1 dykes. **D:** Incompatible trace element diagram showing the island arc tholeiite type trend of the Group 2 dykes. Shaded area is of oceanic arc tholeiites (Pearce, 1983). Thickened pattern is data from Zhao and McCulloch (1993).

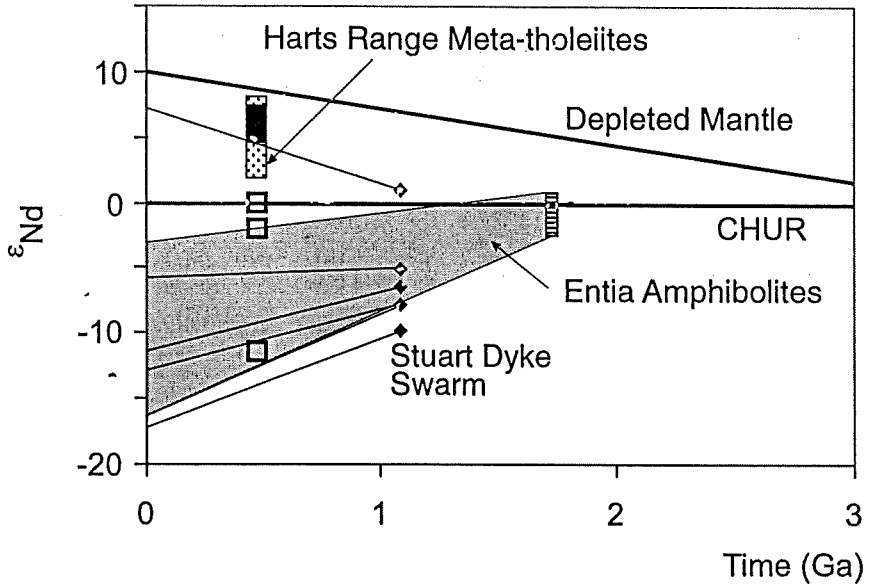

Fig. 9. ε_{Nd} plotted against time for the HRD at 480 Ma. Symbols as for Fig. 5. Also plotted are values for the Harts Range Meta-tholeiites (Sivell and McCulloch, 1991), Entia amphibolites (Foden et al., 1995) and the Stuart Dyke Swarm (Zhao and McCulloch, 1993) projected towards their values at the time of emplacement of the HRD.

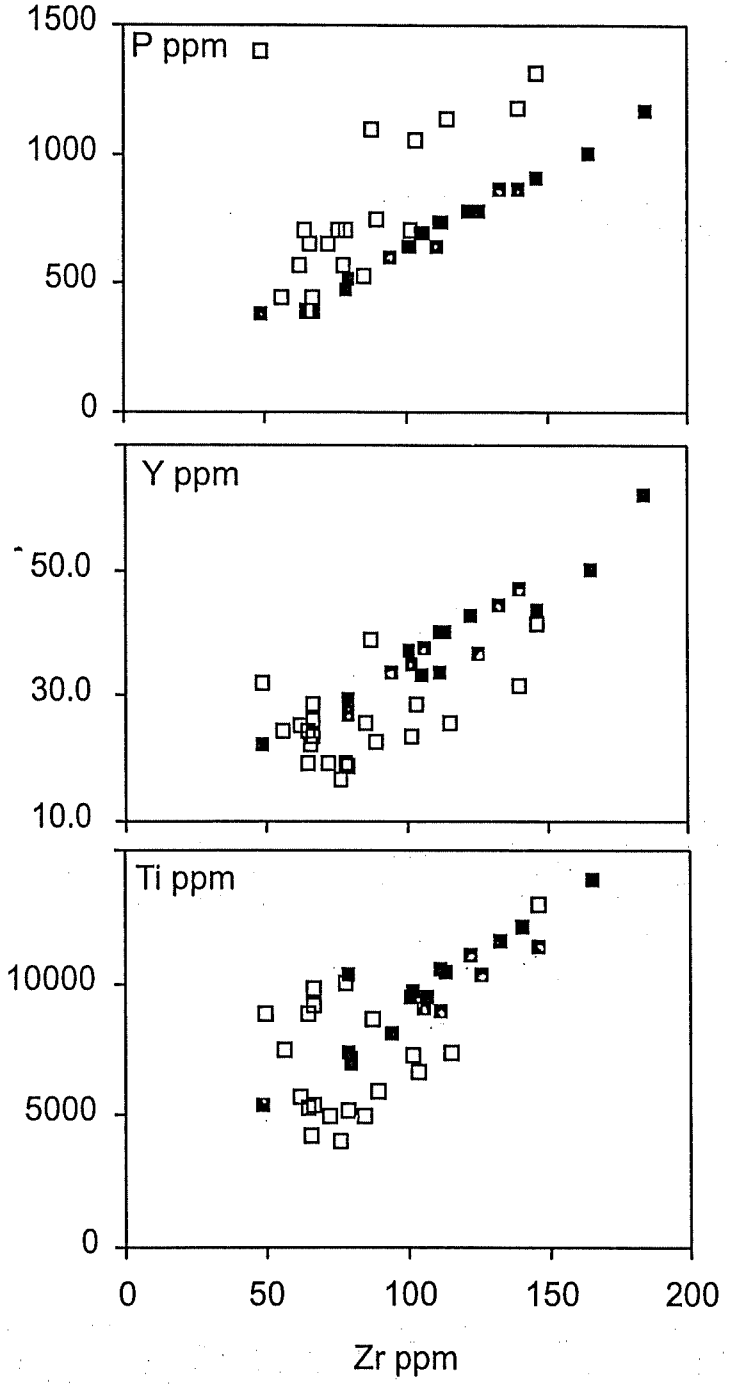

Fig. 10. Plots of incompatible trace elements against Zr, reflecting original igneous fractionation and immobility during metamorphism.

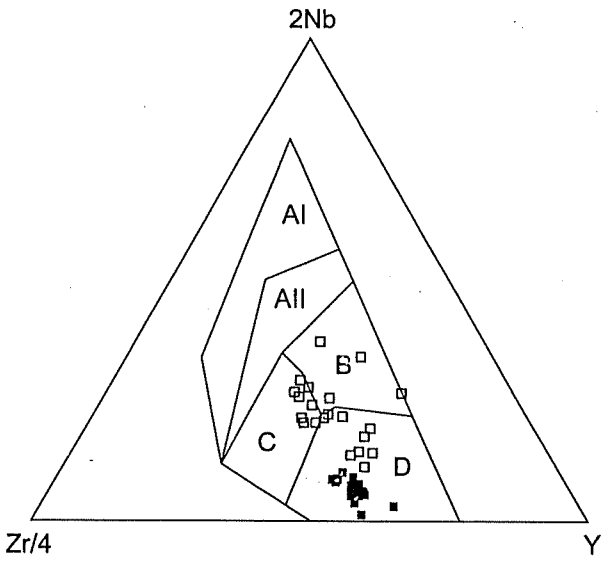

Fig. 11. Zr-Nb-Y discrimination diagram of Meschede (1986): AI, within-plate alkali basalts; AII, within-plate alkali basalts and within-plate tholeiites; B, E-type MORB; C, within-plate tholeiites and volcanic-arc basalts; D, N-type MORB and volcanic-arc basalts. Symbols as for Fig. 5.

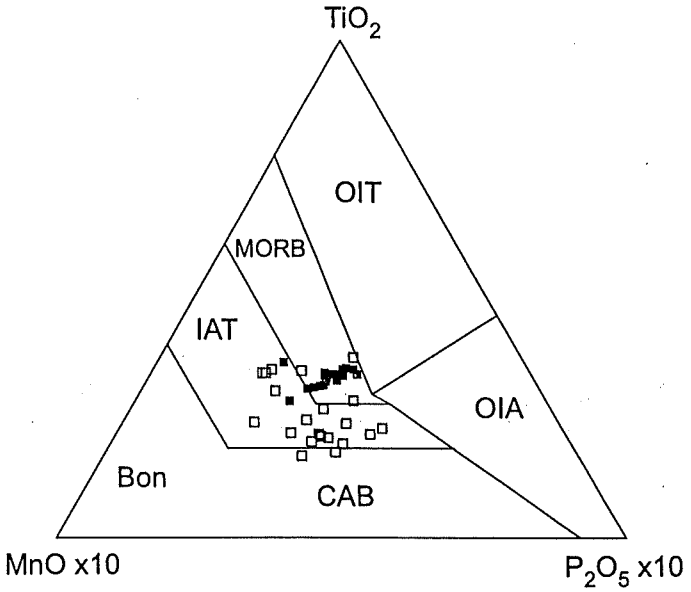

Fig. 12. MnO-TiO2-P2O5 discrimination diagram of Mullen (1983). The fields are: OIT, ocean-island tholeiites; OIA, ocean-island alkali basalts; CAB, island-arc calc-alkaline basalts; Bon, boninite; MORB. Symbols as for Fig. 5.

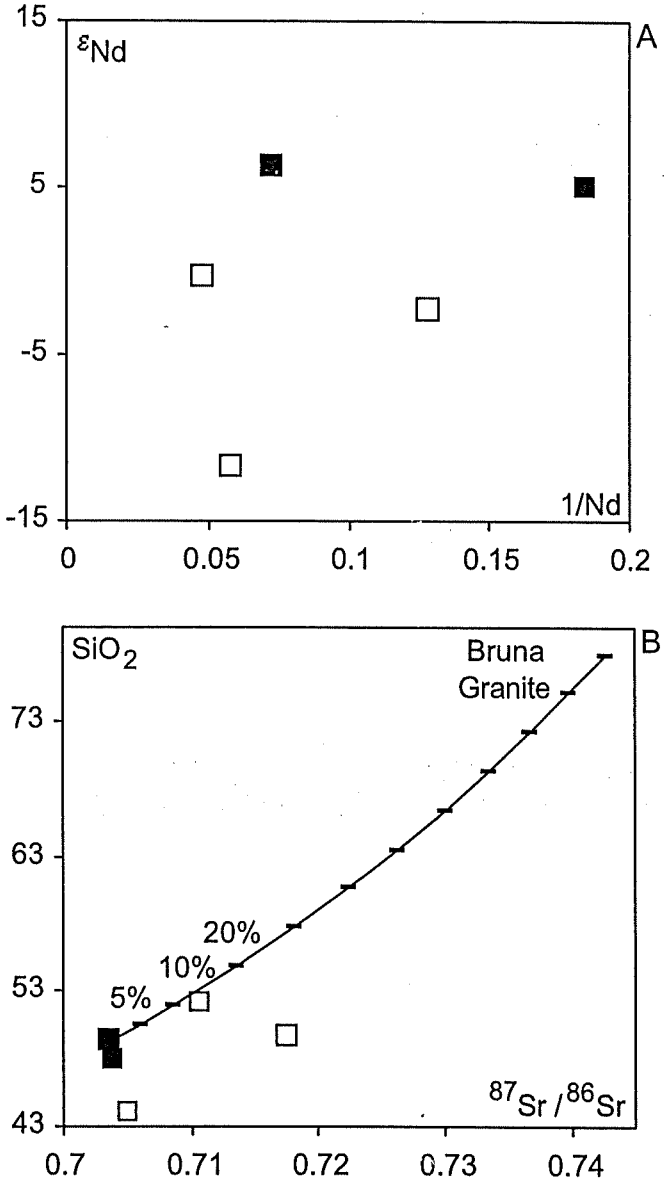

Fig. 13. **A**: ε_{Nd} versus 1/Nd, indicating a broadly positive trend. **B**: Plot of SiO_2 against Sr-isotope ratios illustrating a positive linear correlation. Also plotted is the calculated mixing trend between the Bruna Granite and the most primitive Harts Range Dyke (Group 1). Symbols as for Fig. 5.

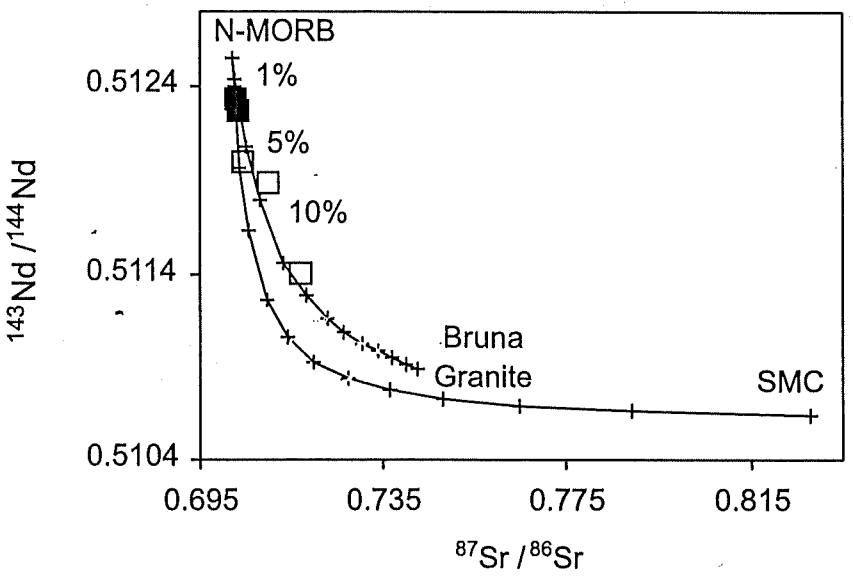

Fig. 14. Simple two component (Nd- and Sr-isotopic compositions) mixing between N-type MORB and the Bruna Granite or calc-silicates from the Strangways Metamorphic Complex (SMC). Symbols as for Fig. 5.

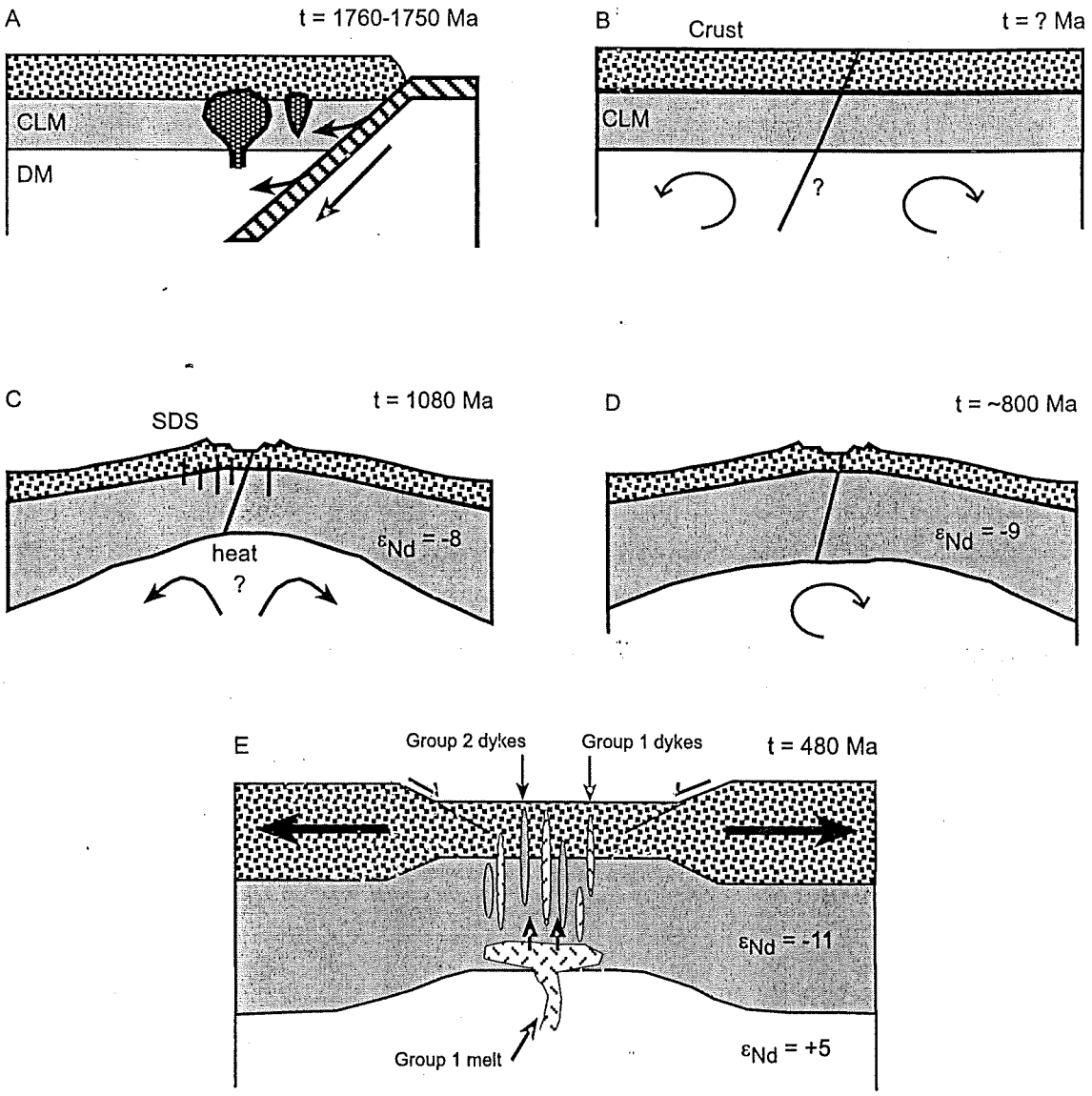

Fig. 15. Schematic model, adapted from Zhao and McCulloch (1993), which illustrates the formation, evolution and coexistence of both the depleted and enriched Harts Range Dykes. DM = depleted mantle, CLM = continental lithospheric mantle.

APPENDIX A

Table A

Pressure - temperature conditions derived using THERMOCLAC v3.0 (Powell and Holland, 1988).

Sample	*T* (°C)	*P* (kbar)	*f*	*cor*	Mineral end-members used
LAD42	738 ± 34	7.9 ± 0.9	0.69	0.464	alm-py-gr-spess-di-hed-cats-ens-fs-tr-fact-ts-parg-an-ab-ilm-geik-pyr-qtz-H_2O
NHRD7A	683 ± 27	7.2 ± 0.8	0.95	0.476	alm-py-gr-spess-di-hed-cats-ens-fs-tr-fact-ts-parg-an-ab-ilm-geik-pyr-qtz-H_2O
LAD6A	741 ± 32	8.0 ± 0.9	0.50	0.453	alm-py-gr-spess-di-hed-cats-ens-fs-tr-fact-ts-parg-an-ab-ilm-geik-pyr-qtz-H_2O
LAD1	718 ± 31	8.2 ± 0.8	1.09	0.486	alm-py-gr-spess-di-hed-cats-ens-fs-tr-fact-ts-parg-an-ab-ilm-geik-pyr-qtz-H_2O
LAD6	705 ± 30	9.1 ± 1.0	1.12	0.473	alm-py-gr-spess-di-hed-cats-ens-fs-tr-fact-ts-parg-an-ab-ilm-geik-pyr-qtz-H_2O

APPENDIX B

Table B
Mineral analysis from representative HRD.

Mineral:	cpx	gt	hbd	ilm	opx	plag	cpx	gt	hbd	ilm	opx	plag	cpx	gt	hbd	ilm	opx	plag
Sample:	LAD42	LAD42	LAD42	LAD42	LAD42	LAD42	NHRD7A	NHRD7A	NHRD7A	NHRD7A	NHRD7A	NHRD7A	LAD6A	LAD6A	LAD6A	LAD6A	LAD6A	LAD6A
SiO_2	51.99	37.95	43.01	0.05	51.23	54.99	50.81	37.70	42.61	0.00	51.30	53.85	51.82	38.38	45.08	0.03	51.88	55.72
TiO_2	0.08	0.06	1.59	51.68	0.06	0.00	0.31	0.04	1.47	53.18	0.06	0.04	0.18	0.04	1.56	52.06	0.03	0.06
Al_2O_3	1.34	21.46	11.87	0.01	0.97	27.91	1.95	21.23	12.13	0.02	0.80	28.04	1.49	21.58	10.43	0.00	0.78	27.99
Cr_2O_3	0.00	0.00	0.00	0.00	0.00	0.00	0.00	0.02	0.00	0.00	0.00	0.00	0.02	0.00	0.00	0.00	0.04	0.01
Fe_2O_3	1.71	2.08	1.59	1.69	1.58	0.11	2.03	2.00	0.07	0.12	1.76	0.10	1.73	1.20	2.37	1.30	1.10	0.10
FeO	7.17	24.96	13.26	44.00	25.84	0.00	8.63	25.36	13.09	44.86	24.51	0.00	7.57	25.01	10.66	44.89	23.48	0.00
MnO	0.13	1.10	0.09	0.41	0.45	0.00	0.24	0.87	0.06	0.30	0.17	0.00	0.18	0.97	0.09	0.35	0.39	0.00
MgO	13.25	5.08	10.76	1.01	19.30	0.00	12.45	5.34	11.15	1.47	20.29	0.00	13.29	6.14	13.00	0.85	21.11	0.00
CaO	23.16	7.97	11.50	0.25	0.46	10.58	22.49	7.30	12.02	0.03	0.41	11.21	22.65	7.02	11.51	0.07	0.44	10.27
Na_2O	0.35	0.02	1.43	0.00	0.00	5.21	0.25	0.00	1.32	0.00	0.00	5.04	0.36	0.00	1.43	0.00	0.00	5.52
K_2O	0.01	0.00	0.78	0.00	0.01	0.14	0.00	0.00	1.30	0.00	0.01	0.18	0.00	0.00	0.49	0.00	0.00	0.07
Total	99.19	100.68	95.88	99.10	99.90	98.94	99.16	99.86	95.22	99.98	99.31	98.46	99.29	100.34	96.62	99.55	99.25	99.74
Si	1.96	2.95	6.48	0.00	1.95	2.50	1.93	2.96	6.47	0.00	1.96	2.47	1.95	2.98	6.65	0.00	1.97	2.51
Ti	0.00	0.00	0.18	0.98	0.00	0.00	0.01	0.00	0.17	1.00	0.00	0.00	0.01	0.00	0.17	0.99	0.00	0.00
Cr	0.06	1.97	2.11	0.00	0.04	1.50	0.09	1.96	2.17	0.00	0.04	1.52	0.07	1.97	1.81	0.00	0.04	1.49
Al	0.00	0.00	0.00	0.00	0.00	0.00	0.00	0.00	0.00	0.00	0.00	0.00	0.00	0.00	0.00	0.00	0.00	0.00
Fe^{3+}	0.05	0.12	0.18	0.03	0.05	0.00	0.06	0.12	0.01	0.00	0.05	0.00	0.05	0.07	0.26	0.03	0.03	0.00
Fe^{2+}	0.23	1.62	1.67	0.93	0.82	0.00	0.27	1.66	1.66	0.94	0.78	0.00	0.24	1.62	1.31	0.95	0.74	0.00
Mn	0.00	0.07	0.01	0.01	0.02	0.00	0.01	0.06	0.01	0.01	0.01	0.00	0.01	0.06	0.01	0.01	0.01	0.00
Mg	0.74	0.59	2.42	0.04	1.10	0.00	0.70	0.62	2.52	0.06	1.15	0.00	0.75	0.71	2.86	0.03	1.19	0.00
Ca	0.93	0.66	1.86	0.01	0.02	0.52	0.91	0.61	1.95	0.00	0.02	0.55	0.91	0.58	1.82	0.00	0.02	0.50
Na	0.03	0.00	0.42	0.00	0.00	0.46	0.02	0.00	0.39	0.00	0.00	0.45	0.03	0.00	0.41	0.00	0.00	0.48
K	0.00	0.00	0.15	0.00	0.00	0.01	0.00	0.00	0.25	0.00	0.00	0.01	0.00	0.00	0.09	0.00	0.00	0.00
Sum	4.00	8.00	15.48	2.00	4.00	4.98	4.00	8.00	15.60	2.00	4.00	5.00	4.00	8.00	15.39	2.00	4.00	4.99

Table C
Mineral analysis from representative HRD cont/d.

Mineral:	cpx	gt	hbd	ilm	opx	plag	cpx	gt	hbd	ilm	opx	plag
Sample:	LAD1	LAD1	LAD1	LAD1	LAD1	LAD1	LAD6	LAD6	LAD6	LAD6	LAD6	LAD6
SiO_2	51.93	38.14	43.72	0.05	52.36	47.31	52.11	38.32	45.53	0.02	52.14	59.00
TiO_2	0.19	0.03	1.52	51.20	0.03	0.00	0.05	0.00	1.31	52.19	0.06	0.00
Al_2O_3	1.86	21.74	11.79	0.00	0.98	32.74	0.94	21.60	10.08	0.01	0.87	24.17
Cr_2O_3	0.00	0.00	0.00	0.00	0.00	0.01	0.02	0.00	0.00	0.00	0.00	0.04
Fe_2O_3	1.70	0.39	1.63	0.00	0.00	0.28	1.75	0.78	1.47	0.00	0.13	0.27
FeO	6.17	24.64	12.18	44.34	23.58	0.00	5.63	23.89	8.38	43.67	22.32	0.00
MnO	0.15	1.30	0.12	0.37	0.37	0.02	0.09	0.54	0.03	0.25	0.19	0.00
MgO	13.79	5.75	11.55	0.54	20.77	0.00	14.52	7.02	14.52	1.47	22.04	0.14
CaO	22.61	7.31	11.42	0.05	0.54	16.65	23.02	6.90	11.89	0.10	0.41	7.34
Na_2O	0.48	0.00	1.75	0.00	0.00	1.92	0.25	0.00	1.12	0.00	0.00	7.48
K_2O	0.06	0.02	0.52	0.00	0.01	0.00	0.03	0.01	0.69	0.00	0.02	0.09
Total	98.94	99.32	96.20	96.55	98.64	98.93	98.41	99.06	95.02	97.71	98.18	98.53
Si	1.95	2.99	6.52	0.00	1.99	2.19	1.96	2.99	6.74	0.00	1.98	2.68
Ti	0.01	0.00	0.17	1.00	0.00	0.00	0.00	0.00	0.15	1.00	0.00	0.00
Cr	0.08	2.01	2.07	0.00	0.04	1.79	0.04	1.98	1.76	0.00	0.04	1.29
Al	0.00	0.00	0.00	0.00	0.00	0.00	0.00	0.00	0.00	0.00	0.00	0.00
Fe^{3+}	0.05	0.02	0.18	0.00	0.00	0.01	0.05	0.05	0.16	0.00	0.00	0.01
Fe^{2+}	0.19	1.61	1.52	0.96	0.75	0.00	0.18	1.56	1.04	0.93	0.71	0.00
Mn	0.01	0.09	0.02	0.01	0.01	0.00	0.00	0.04	0.00	0.01	0.01	0.00
Mg	0.77	0.67	2.57	0.02	1.18	0.00	0.82	0.82	3.20	0.06	1.25	0.01
Ca	0.91	0.61	1.83	0.00	0.02	0.83	0.93	0.58	1.89	0.00	0.02	0.36
Na	0.04	0.00	0.51	0.00	0.00	0.17	0.02	0.00	0.32	0.00	0.00	0.66
K	0.00	0.00	0.10	0.00	0.00	0.00	0.00	0.00	0.13	0.00	0.00	0.01
Sum	4.00	8.00	15.48	2.00	3.99	4.99	4.00	8.00	15.38	2.00	4.00	5.01

APPENDIX C

Table D
Mineral names and abbreviations.

Mineral	Abbreviation	Mineral	Abbreviation
Albite	ab	Hedenbergite	hed
Almandine	alm	Hornblende	hbd
Anorthite	an	Ilmenite	ilm
Ca-tshermaks	cats	Orthopyroxene	opx
Clinopyroxene	cpx	Pargasite	parg
Diopside	di	Plagioclase	plag
Enstatite	en	Pyrope	py
Ferroactinolite	fact	Pyrophanite	pyr
Ferrosilite	fs	Quartz	qtz
Garnet	gt	Spessatine	spess
Geikielite	geik	Tremolite	tr
Grossular	gr	Tshermakite	ts

APPENDIX D

Table E

Dyke sample locations

Sample No.	GPS Location E (05 prefix)	N (74 prefix)
LaD-1	08561	18365
LaD-3	08509	18361
LaD-5	08506	18345
LaD-6	08535	18323
LaD-11	08611	18230
LaD-14	08663	18234
LaD-19	08815	18286
LaD-21	08828	18213
LaD-21-1	08813	18210
LaD-27	08718	18180
LaD-28	08697	18178
LaD-29	08678	18190
LaD-32	08846	18171
LaD-36	08765	18181
LaD-39	08140	18072
LaD-42	08808	18070
LaD-43	08871	18041
LaD-2A	08011	16258
LaD-4A	08024	16257
LaD-6A	08032	18261
LaD-10A	08116	18280
LaD-12A	08100	18339
LaD-14A	08120	18343
GH-2	08000	18295
GH-4	08090	18128
GH-5	07943	18194
GS-1	04638	20119
GS-4	05231	19718
GS-5	05283	19737
GS-6	05307	19833
GS-7	05363	19974
MD-1A	08503	19051
MD-8	08625	18255
NHRD	91730	50900
NHRD-5	91643	50810
NHRD-6	91630	50742
NHRD-7	91598	50688
NHRD-7A	91549	50632
NHRD-9	91434	49877
NHRD-10A	90660	49760
NHRD-10B	90672	49752

Locations are within 5m errors, due to GPS drift